Decoding T Cell Responses to Herpes Simplex Virus Infection in Skin Using Highly Multiplexed Tissue Imaging

Amanda Karin Stole Yeckel

A thesis

submitted in partial fulfillment of the

requirements for the degree of

Master of Science

University of Washington

2024

Committee:

Jia Zhu

Stephen Polyak

Julia Sidorova

Program Authorized to Offer Degree:

Laboratory Medicine & Pathology

University of Washington

Abstract

Decoding T Cell Responses to Herpes Simplex Virus Infection in Skin Using Highly Multiplexed Tissue Imaging

Amanda Karin Stole Yeckel

Chair of the Supervisory Committee:
Jia Zhu
Department of Laboratory Medicine & Pathology

Herpes Simplex Virus (HSV) is a prevalent global health concern, with two main subtypes, HSV-1 and HSV-2, infecting billions of people. While HSV-1 typically causes cold sores and HSV-2 is associated with genital herpes, both can manifest in various forms. Infections often result in painful lesions, but many remain asymptomatic. Immunocompromised individuals face severe complications, including increased susceptibility to HIV infection. HSV establishes latency in neurons, periodically reactivating to cause viral shedding. Most reactivations are subclinical, contributing to the high global prevalence of HSV. Despite ongoing research, there is no cure or vaccine available. T cells play a crucial role in controlling HSV infections, with tissue-resident memory cells (TRMs) influencing reactivation frequency. Chronic infections can lead to T cell exhaustion, characterized by diminished effector functions and memory T cell development, leading to an inadequate immune response. Our study examined T cell responses in HSV-infected skin, exploring activation, exhaustion, regulation, and survival during lesion healing. Using advanced imaging and machine learning techniques, we observed a shift from activated T cells to TRMs post-healing. Additionally, regulatory T cell density was elevated in patients with higher shedding rates. Currently, there is no vaccine available to prevent HSV infection and transmission. However, a deeper understanding of T cell dynamics during lesion healing has the potential to directly guide vaccine development efforts aimed at leveraging T cell responses for effective prevention.

Table of Contents

List of Tables

List of Figures

Acknowledgements

I wish to extend my heartfelt gratitude to my thesis committee, Jia, Steve, and Julia, for their invaluable feedback and guidance during the completion of my master's thesis. Their support has played a pivotal role in shaping the trajectory of my research and elevating its quality. A special shoutout goes to Jia, my thesis mentor, for her kindness and willingness to navigate me through the process, exchanging ideas back and forth to ensure the clarity and coherence of my assertions.

Special thanks to K for his exceptional expertise and unwavering support in the Zhu lab at Fred Hutch Cancer Center. His guidance and assistance, particularly in running the Cellpose analyses, have been indispensable to the success of this project.

I am also deeply grateful to Eirini at the Hutch for generously sharing her expertise and insights, which proved invaluable in exploring additional cell segmentation options for my research.

I extend my heartfelt appreciation to The Department of Laboratory Medicine & Pathology and all attendees of my clinical research conference presentations for their engaging questions and constructive feedback. Their contributions have significantly enriched my work.

I am indebted to my family for their unwavering support and encouragement throughout this journey. Their insightful questions and genuine interest in my research have been a constant source of motivation.

I extend a special appreciation to my husband, David, for his limitless patience and steadfast support. His willingness to sit through countless rehearsals of my presentations has been immeasurably valuable.

Lastly, I would like to thank all those who have contributed to this thesis in ways both big and small. Your support and encouragement have been crucial in making this endeavor possible. Thank you all for believing in me and being a part of this incredible journey.

Thesis Chapters & Descriptions

Chapter	Description
Chapter 1	**Herpes Simplex Virus: Silent but prevalent spread** This chapter provides an introduction and background information on Herpes Simplex Viruses type 1 and 2 which cause Herpes in humans, including epidemiology, diagnosis, treatment, complications, and pathology.
Chapter 2	**The Importance of T cells: Immune response to Herpes Simplex Virus infection** This chapter reviews the role of skin and immune cells in combatting Herpes Simplex Virus infection and addresses the importance of T cells. Immune exhaustion and activation is defined and discussed, with particular emphasis on T cells.
Chapter 3	**Delving Deeper: Highly Multiplexed Tissue Imaging (HMTI)** This section introduces Highly Multiplexed Tissue Imaging (HMTI) technology compared to more simplistic methods like immunofluorescence (IF) and immunohistochemistry (IHC) staining. This section focuses primarily on the multiplexed method used for this project, which is Chip Cytometry.
Chapter 4	**Cellpose: a machine learning-based cellular segmentation algorithm** This chapter describes a machine learning algorithm used for segmenting cells in fluorescently-stained tissue images. Cellpose was used to identify and quantify specific cell types within the tissue samples used in this study.
Chapter 5	**Methods** This chapter outlines the methods used to achieve results. Included in this section are subject demographics and sample preparation information. Cellpose was used for quantitative output of cell segmentation. ImageJ/Fiji was used for raw image cleaning, splitting, and merging.
Chapter 6	**Results & Discussion** This chapter presents experimental findings, both qualitative and quantitative, and discusses interpretation of those results.
Chapter 7	**Conclusion** This chapter offers a condensed overview of the findings, constraints, suggestions for future research, and the importance of the study.

Chapter 1 – Herpes Simplex Virus: silent but prevalent spread

HSV intro, complications, & public health importance

Herpes Simplex Virus (HSV) is a common public health concern, in fact, it is the most common ulcerative sexually transmitted infection (STI) in the developed world [25]. HSV infections in humans can manifest as painful, recurrent blisters on oral or genital mucosa, but most infections are subclinical [53], [29], [17], [58], resulting in silent spread throughout the population. Women are at higher risk of acquiring HSV-2 than are men [13]. Although HSV may appear less sinister than other infectious diseases, it comes with serious risks and complications, including death in immunocompromised populations [29], [5], [9], [17]. Repeated HSV-1 reactivation has been implicated in the pathogenesis of Alzheimer's disease and amnestic mild cognitive impairment [32]. Additionally, people infected with HSV have increased risk of blindness caused by stromal keratitis [53], central nervous system diseases [64], herpes simplex encephalitis [32] and an increased risk of HIV transmission [53] and acquisition [13], [8], [65], [31], [57]. The increased risk of HIV-1 acquisition is due to the CD4+ T cell infiltration in the upper dermis, providing HIV-1 with a vast number of target cells [65]. As a result, tissue in healed lesion areas of the skin are much more susceptible to HIV infection compared to non-lesion areas [65]. CD4+ T cell proximity to dendritic cells (DCs) can further enhance the risk since DCs activate T cells [65].

HSV types, manifestation, and public health impact

There are two subtypes of Herpes Simplex Virus that infect humans. These are closely related double stranded DNA viruses [17] of the human Herpesviridae family, with some notable differences. Approximately 70% of the global population is infected with HSV-1 [64], [17] whereas about 15% are infected with HSV-2 [25]. HSV-1 commonly manifests as blisters around the mouth but can also result in genital herpes lesions [26], [64]. HSV-2 is associated with genital herpes [17] and is typically more severe, with a greater likelihood of subsequent reactivations than HSV-1 [25]. Most people infected with HSV do not display symptoms [53], [57]. Therefore, it is unsurprising that studies show that 10-25% of people infected with HSV-2 are unaware that they have genital herpes [17]. Most viral transmission occurs during periods of subclinical shedding [17], [59], or when people are symptom-free.

Mechanism of infection and transmission

HSV is a lifelong infection without a cure [17]. The virus enters the body via skin-to-skin contact with herpesvirus lesions or genital secretions that contain the virus. HSV initially infects the epidermal epithelial cells, replicates within them causing ulcerative skin lesions, and then is transported via the sensory nerves to establish latency in the sensory neurons [35], [26]. HSV-1 establishes latency in the trigeminal ganglia and HSV-2 in the dorsal root ganglia [37], [29]. Subsequent reactivations are typically milder and less frequent over time than the primary infection [17], [25]. HSV can be transmitted horizontally (from sexual contact) or vertically (from mother to neonate) [58].

Asymptomatic (in the absence of herpetic lesions) viral shedding accounts for 50-80% of reactivations [67], resulting in effective spread of HSV throughout the population. Subclinical shedding accounts for one third of the total days of a reactivation [58]. Several factors impact HSV shedding rates. Increased subclinical shedding rates result in people with more recent HSV acquisition [58] and in those infected with both HSV-1 and -2 compared to just HSV-1 [58]. A large variability in shedding rates has been observed between patients and *Schiffer et al* (2010) characterized some factors that influence viral titer shedding rate using a mathematical model of HSV-2 shedding. It was found that increased CD8+ T cell density at the lesion site correlates with a decrease in infected cell lifespan [47]. Rate of containment of infection by the peripheral immune system is the primary driver of severity and duration of HSV-2 reactivation [47]. Additionally, closer proximity of CD8+ T cells to infected cells decreased HSV-2 shedding [47].

Diagnosis, symptoms, treatment, & therapeutic development

Herpes infection is diagnosed by clinical evaluation of characteristic skin lesions, confirmed with serological testing of the vesicle fluid [17], [25]. Skin lesions appear 4-7 days post-infection and can coalesce into ulcers before healing [17]. Approximately a third of individuals with HSV-1 or -2 experience painful, recurrent blisters that result from viral reactivation [53]. Lesions manifest as tightly clustered, fluid-filled bumps, containing inflammatory cells, virions and cellular debris [17]. Lesions last between 7 and 10 days and typically occur in and around the genitals, eyes, mouth, and lips [25]. Ulcerative lesions can last several days and viral titer and length of viral shedding correlate with the severity of symptoms [35]. Lesions on mucosal surfaces appear to form ulcers immediately, bypassing the pustule phase in non-mucosal areas [17]. Primary genital

manifestations of HSV-1 and HSV-2 are indistinguishable by appearance, and therefore, must be delineated via Type-specific IgG serology testing [17]. Common symptoms accompanying these characteristic skin lesions include dysuria (pain with urination), headache, malaise, fever, headache and body aches [17]. Antiviral medications can be used to manage severe symptoms and reduce the risk of HSV transmission between partners [17], but currently there is no vaccine or cure for HSV. Antiviral treatment, mainly Acyclovir, can lessen the severity of disease symptoms by reducing shedding [25] if necessary. While antiviral therapy can reduce the transmission risk of HSV, it does not lower the risk of HIV-1 transmission or acquisition in HSV-2+ individuals [8], [7], [65]. Topical antiviral treatments are discouraged as they are largely ineffective [25].

In summary, the current state of managing herpesvirus symptoms and spread in humans is antiviral therapy and prevention. Prevention can be challenging since abstaining from intercourse does not guarantee protection as virus can be shed from skin in non-genital areas. The best course of action is to focus on vaccine development, likely involving T cells. Since T cells, specifically CD8+ T cells, are responsible for controlling recurrent infections locally, a more comprehensive understanding of these T cell populations and their role in controlling infection could contribute to advancements in prophylactic development.

Chapter 2 – The importance of T cells: immune response to HSV infection

Immune cell response to HSV infection

Many immune cell types are involved in inhibiting HSV infection in the skin. The skin biopsies used in this project include the epidermis (top layer), the dermis (vascularized mid-layer) and the dermal-epidermal junction (DEJ), which serves as an interface between the dermis and epidermis [1]. CD8+ memory T cells have been found to reside at the DEJ, ready to swiftly react to invading pathogens [44], [35]. After HSV infects the skin, innate immune cells are likely first to respond, followed by CD4+ and CD8+ T cells. Langerhans Cells (LCs), known as dendritic cells of the skin [63], and other Dendritic Cells (DCs) act as gatekeepers in the skin [27], [26]. Plasmacytoid dendritic cells (pDC) are also an important part of the innate immune cell response to HSV infection. In normal, non-inflammatory conditions, pDCs are only found circulating in the blood and lymph nodes, but in inflammatory states they can be seen in the skin [11]. pDCs contribute to the control of HSV infection by stimulating T cell proliferation [11]. HSV-specific T cells are essential for viral clearance of the pathogen [53].

T cell response

Cytotoxic (or CD8+) T cells kill infected cells, whereas helper (or CD4+) T cells indirectly kill target cells by directing cytotoxic T cells and other immune effector cells to kill. CD4+ T cells respond first to infection, followed by CD8+ T cells [26]. CD4+ T cells are responsible for regulating an effective immune response [64]. Cytotoxic CD8+ T cells are critical in controlling HSV infection and reactivation [66]. HSV-specific CD8+ T cells significantly reduce reactivation by interfering with viral replication and spread. The presence of CD8+ T cells correlates with termination of the infection [26]. However, HSV-1 can still reactivate even in the presence of a large pool of virus-specific CD8+ T cells. This is likely due to the restricted functional nature of the exhausted population [45]. T cells are unable to prevent latent infection or reactivations, suggesting that HSV can modulate T cell function via T cell receptor (TCR) remodeling [53].

Regulatory T cells, or Tregs, have immunoregulatory properties that likely contribute to T cell exhaustion. A reduction in Tregs plus anti-PD-1 blockade showed a synergistic positive effect on reversing T cell exhaustion and controlling viral load [46]. The involvement of Tregs in T cell exhaustion is likely due to the regulatory nature of Tregs, specifically the production of

suppressive cytokines [34]. Treg infiltration to the tissues has been observed during acute infection, which decreases during lesion healing [65]. A higher density Tregs at the time of lesion is associated with higher viral replication and the extent of tissue infiltration correlates with the severity of recurrent lesions [65].

Tissue-Resident Memory (TRM) T cell response

Following antigen presentation by antigen presenting cells (APCs), naïve CD8+ T cells can differentiate into several subtypes, a significant one being Tissue Resident Memory T cells (TRMs) [64], [6]. After clearance of the initial infection, Tissue-resident memory (TRM) CD8+ T cells are found at the epidermis, close to the site of infection [26] and poised to act as first responders to any subsequent reactivating infections [41]. HSV-specific CD8+ T cells persist at the DEJ for up to two months after lesion healing [66]. The frequency and clinical course of infection are determined by presence of persistent HSV-2-specific CD8+ T cells near the site of infection [66]. While no single marker exists to identify TRMs, CD69 is the marker most used for identification [27] and sometimes CD103 [6], [44]. TRMs can be identified by the expression of CD69 in combination with lack of other surface markers, such as LAG-3 and TIM-3, as LAG-3 and TIM-3 are terminal exhaustion markers [6]. TRMs hold promise for development of vaccine therapeutics since they congregate at infection barrier sites for quick response to infection. Protective immunity comes from T cells, and thus, vaccine development should focus on elevating T cell numbers and preventing exhaustion.

T cell activation and exhaustion

Activation

T cells can activate when antigen is present, resulting in TCR stimulation. Activated T cells can express Granzyme B (GZMB), CD69, CD278 (ICOS), and Ki-67 (proliferation).

Granzyme B (GZMB) is a serine protease produced by cytotoxic T cells and NK cells that works in concert with perforin to kill target cells [30]. GZMB expression is typically highest in lesion tissues and is seen at much lower levels in healed or control tissues [10]. CD69 can be used as a marker of early activation in T cells, or it can be an indicator of tissue residency [40], [62], [6]. As previously mentioned, no single marker exists to identify TRM cells. Therefore, their function must be inferred from contextual clues and combinations of CD69 with the absence of

other surface markers [6]. Inducible T cell costimulator, ICOS, is a cell surface receptor related to CD28 in structure and function, that is involved in T cell activation and proliferation [3]. Ki-67 is an intracellular marker identifying recent cell proliferation [10].

Exhaustion

When T cells are constantly exposed to antigen, such as in the case of a chronic recurrent viral infection, like HSV, they can become exhausted. Both CD4+ and CD8+ T cells can become exhausted. T cells in an exhausted state are characterized by their diminished effector functions, such as reduced cytokine production, and memory functions, coupled with the persistent expression of inhibitory receptors (IRs) [15], [64], [43]. T cells enter an exhausted state after experiencing TCR overstimulation during prolonged T cell activation [15]. Exhaustion develops in a stepwise progressive manner [60] as a response to chronic infection or cancer. The severity of exhaustion is determined by several factors, such as cytokine levels, duration and magnitude of antigen exposure, access to CD4+ T cell help, and by expression of inhibitory receptors [62].

In our study, we focused on staining for a specific subset of inhibitory receptors commonly expressed by exhausted T cells, which included: T cell immunoglobulin and mucin domain-containing protein (TIM-3), Lymphocyte Activation Gene 3 (LAG-3), and programmed cell death protein 1 (PD-1) [14], [16], [43], [64]. PD-1 and Cytotoxic T-lymphocyte associated protein 4 (CTLA-4) are the most well-studied inhibitory receptors used therapeutically in cancer treatment [24]. Exhaustion is reversible [15] as shown by effective PD-1 blockade therapy for various cancers [46], [3], [34], [20], [45], [43]. Co-blockades of other immune checkpoint inhibitors (CTLA-4, TIM-3, LAG-3, TIGIT, for example) with PD-1 have shown improved outcomes in terms of re-invigorating exhausted T cell function and reducing viral load, compared to just PD-1 blockade alone [24], [60], [45], [46], [3], [34], [20], [48]. This synergistic effect suggests different mechanisms of inhibition from different checkpoints or inhibitory receptors. The sustained expression of inhibitory receptors is a crucial characteristic of T cell exhaustion [34], [43].

PD-1:

PD-1 is the best-characterized inhibitory receptor [15], [62], [46], [34], [43] and is highly expressed on CD8+ T cells during chronic viral infection [3]. PD-1 works by inhibiting effector function and proliferation of T cells [62] by reducing signals downstream of TCR stimulation

[48]. PD-L1, the ligand to PD-1, regulates the extent of inflammation [48]. The co-expression of PD-1 in combination with other inhibitory receptors, such as LAG-3 and TIM-3, adds to the certainty that a T cell is exhausted [46] because PD-1 is also transiently expressed on effector T cells during acute infection [62], [3] and can be detected on the surface of naïve T cells 24 hours after activation, with expression decreasing as antigen is cleared [48]. PD-1 expression then increases again on exhausted cells [3], [46], [34]. The greater number of inhibitory receptors on a cell surface, the more severe the exhaustion [15], [43], [3].

LAG-3:

Similarly to PD-1, LAG-3 is expressed on the surface of newly activated T cells and then equilibrates over time [24], [62]. LAG-3 contributes to exhaustion by inhibiting the TCR signaling itself, and therefore has a synergistic effect when combined with PD-1 blockade [24]. LAG-3 indirectly inhibits effector T cell function by promoting the immunosuppressive properties of Tregs [24], [2]. It dampens the CD4+ T cell response by engaging the MHCII receptor [2]. In addition to T cells, LAG-3 is also expressed on NK cells, B cells, and plasmacytoid dendritic cells (pDCs) [24]. LAG-3 and PD-1 epitopes are more common in symptomatic HSV-1 patients compared to those without symptoms [45]. Levels of LAG-3 appear to spike right after infection and then equilibrate over time [62].

TIM-3:

TIM-3 expression marks the most terminally dysfunctional CD8+ T cells, and therefore, is a more reliable indicator of immune exhaustion than PD-1 [24]. TIM-3 is also expressed in CD4+ Tregs, NK cells and DCs [2], [24]. It can act in an inhibitory manner on DCs by dampening inflammasome activation [24]. On circulating CD4+ Tregs, however, TIM-3 is either expressed at very low levels, or not at all, but expressed at a higher level in tissue-resident Tregs at the site of inflammation [2]. TIM-3, like LAG-3 is often co-expressed with PD-1, but this is not always the case [62]. All virus-specific TIM-3+ CD8+ T cells also co-express PD-1 [2]. Expression levels correlate with the level of exhaustion and severity of disease [62], [60]. However, more research is needed on how the TIM-3 signaling pathway leads to exhaustion [24].

Summary:

To summarize, exhausted T cells are a heterogeneous population defined by their loss of effector functions which include proliferation, memory, and metabolic regulation capabilities [34]. Expression levels of inhibitory receptors change depending on the state of exhaustion. PD-1 and LAG-3 are expressed briefly after T cells become activated, whereas TIM-3 is expressed later on fully differentiated exhausted T cells and identifies the most severely exhausted T cell subsets during chronic viral infections [24]. Since T cell exhaustion is an indicator of poor prognosis in chronic diseases and cancer, a better understanding of T cell exhaustion is crucial for the developing more effective therapeutics.

Thesis statement

The aim of this thesis project is to use highly multiplexed tissue imaging in conjunction with automated cell segmentation to quantify and characterize T cell populations found throughout the lesion healing process in HSV-infected skin lesions. Specifically, the goal is to define these T cell functional states in terms of activation, regulation, and survival (tissue residency).

Chapter 3 – Delving deeper: highly multiplexed tissue imaging

Highly Multiplexed Tissue Imaging (HMTI)

While Immunohistochemistry (IHC) and Immunofluorescence (IF) staining are the most widely accessible methods for labeling antigens in a tissue section, they are limited to only a handful of markers per tissue sample due to spectral overlap [36], [56], [55]. Flow cytometry offers the ability to detect a multitude of biomarkers but lacks spatial distribution data [36]. Highly Multiplexed Tissue Imaging (HMTI), on the other hand, allows for vast combinations of biomarkers to be analyzed on a single sample, plus valuable spatial distribution information to provide a comprehensive view of the tissue microenvironment [55], including information on cell composition, phenotype, and function. "Multiplex" refers to the capability of detecting multiple signals simultaneously and is a powerful tool for both diagnostic and research use. Various multiplexed technologies have entered the market recently, including metal-tagged antibodies, DNA-barcoded antibodies, and fluorescence-conjugated antibodies [52]. Highly multiplexed imaging methods offer the chance to understand better the pathogenesis of complex diseases that would not be feasible with traditional staining methods.

Chip Cytometry

Fluorescent multiplexing technologies use fluorophore-conjugated antibodies for detection of up to 100+ biomarkers [12], [50]. These are arguably the most established methods due to availability of antibodies, instruments, and reagents [12]. Multiplexed fluorescence imaging overcomes the limitation of spectral overlap by using a cyclic staining and bleaching process [12]. Hennig et al [19] first described a chip-based method for repeated cycles of staining, imaging, and bleaching of immobilized cells on a chip.

Chip Cytometry is the fluorescence based HMTI technology used in this study. Chip Cytometry uses repeated rounds of staining with directly-conjugated fluorescent antibodies, up to five at once, allowing many biomarker combinations to be analyzed on a single tissue sample at different times. The high-resolution images produced from Chip Cytometry provide spatial information at the single cell level. Chip Cytometry is validated for use on multiple sample types, including cell suspensions in 2017, fresh frozen in 2019, and FFPE in 2021 [22], [23].

Chip Cytometry process flow

For our fresh frozen skin biopsy samples, a tissue section is affixed to a “chip” which is a microscope slide with a fluidics chamber. An initial background scan is performed to map the location of tissue on the slide and to subtract out any background signal from the marker scan. After antibody staining and washing, the slide is imaged with a fluorescent microscope in tandem with the Chip Cytometry scanning software. In between staining cycles, the sample is photobleached to remove signal from the previous stain. After obtaining the desired biomarkers, images can be exported for third-party use (image cleaning, merging, segmentation).

Benefits & limitations

A major benefit to using Chip Cytometry for multiplexed staining and imaging is that the tissue sample can be preserved for up to two years and reinterrogated with new biomarkers as needed. Additionally, it uses open-source reagents so users can choose to use antibodies they are familiar with. Autofluorescence is subtracted from images using background scans in between each round of staining/imaging. Images produced are 32-bit true color High Dynamic Resolution, allowing high quality downstream image analyses [55].

As with all multiplexing methods, this technology comes with its own set of limitations. While it is possible to do 5-plex staining, you are often limited to a single antibody per round of staining due to the limited availability of directly conjugated antibodies (PE is the most commonly available due to the ease of photobleaching). Additionally, directly conjugated antibodies are less sensitive than indirect antibodies because there is no amplification step. Finally, this system is not fully automated; users must at the machine to run scans, perform antibody staining/washing, and transition between steps.

In essence, Chip Cytometry facilitates the visualization of cell phenotypes, subcellular components, composition, and distribution within tissue.

Figure 1: *Cell phenotype visualization via fluorescent signals generated by Chip Cytometry*

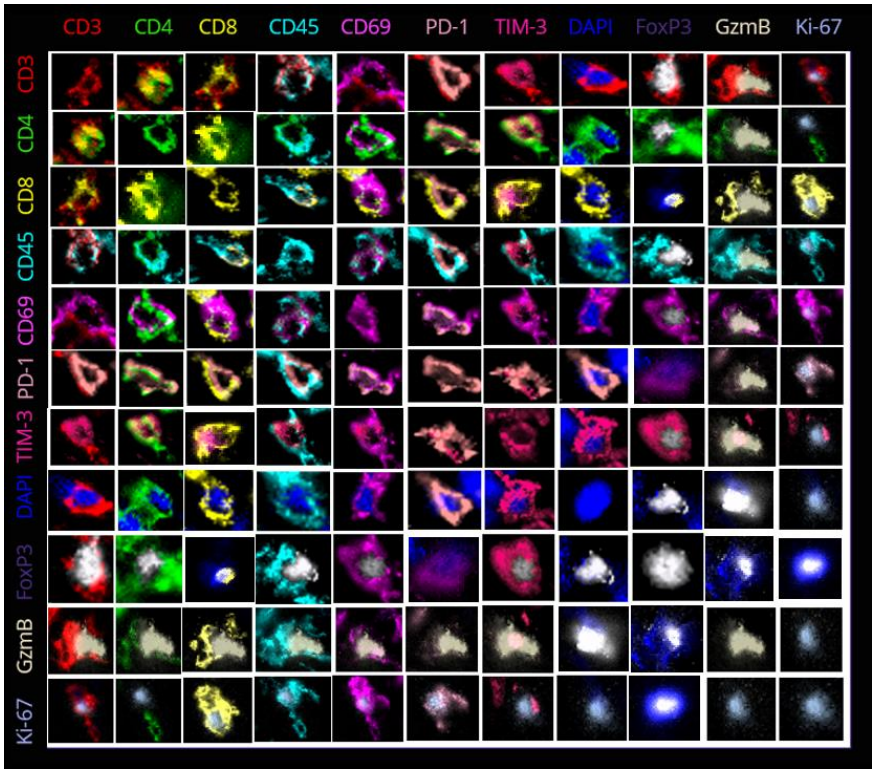

Fig 1: Snapshots of individual cells with various co-expressed marker combinations to illustrate the phenotype and function of immune cells found within skin biopsies. Stained antibodies are specific to CD3, CD4, CD8, CD45, CD69, PD-1, TIM-3, DAPI, FoxP3, GZMB and Ki-67.

Figure 2: *Example Cellpose segmentation for CD8+ T cells*

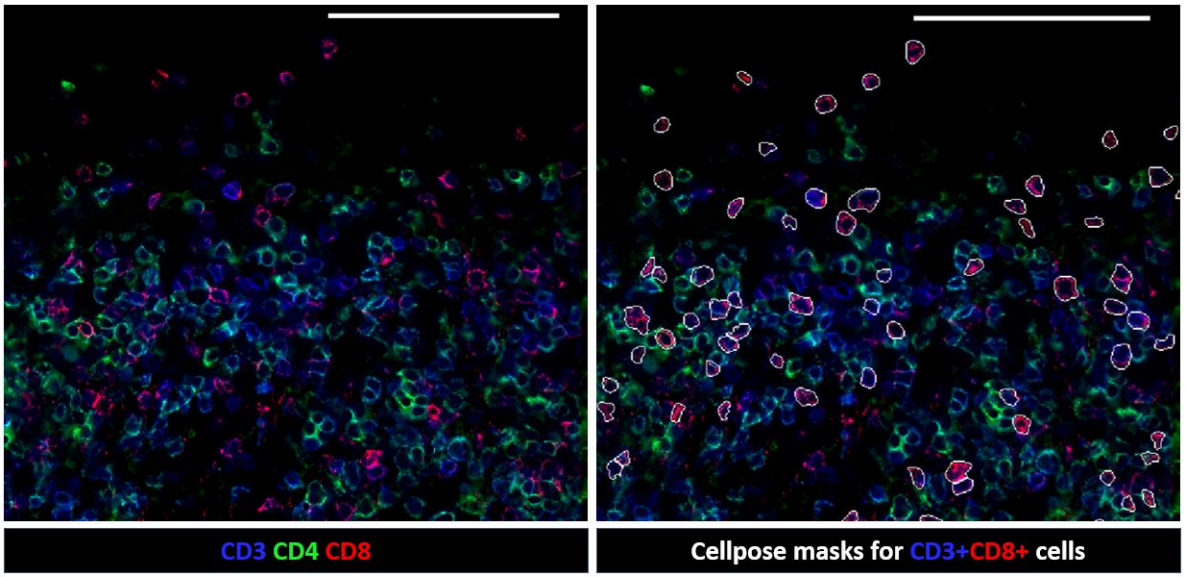

Fig 2: Example Cellpose segmentation for CD8+ T cells from Subject B post-healed tissue biopsy. "Masks" are portions of the image that are isolated from the rest of the image. The image on the left shows marker staining without Cellpose segmentation masks applied and the right image is with Cellpose segmentation masks applied. Scale bar = 100μm.

Cell segmentation is the process of identifying the precise boundary of individual cells in a biological sample, in this case: densely packed tissue sections. Although cell segmentation can be performed manually, this is labor-intensive, not scalable, and introduces bias due to the subjective nature of the task. Manual segmentation can vary considerably between users. The complex patterns derived in the Chip Cytometry approach require sophisticated image analysis, whereby individual cells are identified for counting. Here, I will provide a brief overview of the selected image analysis platform and outline the steps involved in analyzing tissue images generated by Chip Cytometry.

Cell segmentation remains highly challenging in multiplexed image analysis, primarily due to the lack of clearly defined cell borders and the possibility of individual pixels containing data from multiple cells [55]. Segmentation is especially difficult for tissue samples compared to cell suspensions, because there are densely packed and overlapping cells which are hard to distinguish. Another difficulty associated with HSV-infected skin lesions is the presence of a significant infiltration of immune cells, which exhibit varying morphology and size [18].

Depending on where the tissue section is sliced, varied sizes and morphology can be challenging to identify as an individual cell. The Zhu Lab has attempted automated segmentation using the ZellScanner built-in software, but the results for tissue samples were highly inaccurate.

Three approaches for cell segmentation have been discovered to be near human-level approaches in the ability to accurately segment cells: Cellpose, DeepCell/DeepDistance, and Mask R-CNN [18]. All three of these approaches seek to identify whether a pixel belongs inside or outside a cell boundary. Cellpose models the horizontal and vertical gradients within a topological map, characterized by a single smooth basin [Han]. This approach allows for inferring a cell's presence through gradient tracking. Cell detection using DeepCell/DeepDistance involves identifying cell centers and solving this challenge by modeling distances to cell centroids and the nearest cell boundary [18]. Mask R-CNN, a versatile instance segmentation method, utilizes rectangular bounding boxes to delineate individual objects and has been tailored specifically for cell segmentation [18]. High cell density and lower resolution impact these models' success at segmentation. It was found that the prediction performance of Cellpose stands out the most in this experiment of using data sets and training sets of images and before and after further training of the model [18].

Cellpose is an open-access deep learning-based algorithm that can be used for segmentation of cells within tissue. It can precisely segment cells from a wide variety of image types, but it is best suited for fluorescent microscopy images, including those with overlapping and densely packed cells, as seen in tissue. Cellpose was trained on a highly varied dataset of 608 images with over 70,000 segmented objects, including cells with complex shapes as well as non-cell objects [54]. Training dataset images included fluorescence images, brightfield images, membrane-labeled cells, other microscopy, and non-microscopy images. This diverse dataset allows the neural network (the machine learning model) to generalize more broadly and robustly, and it eliminates the need for further model retraining or parameter adjustments. Although the algorithm does not require model retraining, we trained it on additional images to be more specific to the needs of our lab. This was achieved by having several different lab members perform Ground Truths on sample images, meaning they hand-outlined the regions of interest, or the objects we thought were cells. "Ground Truth" refers to the true answer to a specific problem, which in this case is quantifying the various cell shapes found in skin [54]. Brightness,

cell boundary and halo effect are some of the important parameters used to determine which objects are cells. Ground truths masks were done at 400% magnification, grayscale, and optimized brightness [18].

In classical segmentation, the watershed algorithm is commonly used, but it struggles with cell types having multiple intensity basins. To address this, a neural network based on the U-Net architecture was trained to predict gradients on a topological map, creating vector fields. These fields were used to route pixels to the center of each cell, enabling precise visualization of individual cells and their shapes. [38].

The original release of Cellpose is a generalist model approach that can be applied to segmenting a wide variety of biological images. However, given the variation in segmentation styles, applying a general approach to all images may not yield the best performance on all images [Han]. Cellpose 2.0 introduces two models fine-tuned with data from TissueNet and LiveCell. These models enhance the mean average precision (mAP) for TissueNet and LiveCell test images to approximately 0.75 and 0.7, respectively. The model can segment cells based on either nuclei or intracellular markers as it is agnostic between cells and nuclei [18].

Cellpose 2.0 introduces the concept of "human-in-the-loop" training, whereby users actively participate in refining the algorithm to suit their dataset. This version maintains the same neural network architecture but offers various segmentation styles for users to evaluate and select the most suitable for their training datasets [18]. "Human-in-the-loop" training involves correcting an imperfect model using human feedback, which is then incorporated back into the algorithm to enhance its performance. This approach proves beneficial in optimizing the algorithm to specific datasets, considering the substantial variability in human annotation. Additionally, this release necessitates less training data and reduces annotation times by incorporating the "human-in-the-loop" methodology.

Chapter 5 – Methods

Patient demographics and biopsy collection

Adults who were both in good health and tested positive for HSV-2 were enlisted from the University of Washington Virology Research Clinic in Seattle, WA. The HSV-2 status was determined using Western blot analysis, as explained in previous studies [28]. All participants were confirmed to be HIV-negative, and biopsy procedures were carried out according to established methods [66], [42]. The research protocol received approval from the University of Washington Human Subjects Review Committee, and all participants provided written consent. Biopsies with a diameter of three millimeters were taken during clinical recurrences from sites with active lesions. Similarly, biopsies were also collected at the same sites after the lesions had healed, following previously established procedures [66], [67], [40]. Biopsies from acute lesions covered half of the vesicle area and the other half covered the immediately adjacent erythematous skin area. Biopsies from the post-healing period were obtained from the predominant lesion area, typically contiguous to the previous biopsy site. Control skin biopsies were taken from normal, epithelialized inner arm skin, and/or the contralateral anatomical site of HSV reactivation (**Table 1**).

Table 1: Subject demographics from which skin punch biopsies were obtained

ID	Subject ID	Biopsy type	Sex	HSV-1/2 status	Age	Years with HSV	Lesion site	Shedding activity[d]
A	9149	Lesion, healed	F	HSV-2	53.3	29.46	Perineal	24%
		Lesion, 8wph[a]						
B	13279	Lesion, healed[b]	F	HSV-1&-2	47.9	26.78	Perineal	5%
		Lesion, 9wph						
C	15146	Lesion, healed	F	HSV-2	62.2	40.83	Buttock	53%
		Lesion, 8wph						
D	10110	Lesion, healed	F	HSV-1&-2	39.3	1.58	Labia	31%
		Lesion, 2wph						
		Lesion, 4wph						
		Lesion, 8wph						
		Control[c], 8wph						

[a]**wph** = weeks post healed

[b]**healed** = lesions are considered "healed" when the lesion site skin re-epithelializes and there is no longer visible damage to the tissue

[c]**control** = the control sample is a contralateral tissue biopsy taken from the inner arm (non-lesioned area), at the 8 weeks post healed timepoint

[d]**percent HSV shedding activity** determined by PCR

HSV detection in biopsy tissues

All collected tissue samples were fresh frozen in an optimal cutting temperature (OCT) compound and stored at -80°C until further processing. Immunofluorescence staining was conducted using a rabbit polyclonal antibody (Agilent, Cat# B0116, RRID: AB_2335703) to identify HSV-1 & HSV-2 antigens in biopsies from skin lesions. For each biopsy, DNA was extracted from six 8-µm thick tissue sections. A highly sensitive PCR assay [33] was used to detect HSV-1 and HSV-2 DNA in both lesion and post-healed biopsies, serving the dual purpose of virus quantification and screening for subclinical shedding.

Cyclic immunofluorescence staining and image acquisition using Chip Cytometry

Equipment & materials:

- ZKW wash buffer (or Phosphate Buffered Saline, PBS)
- ZKW storage buffer
- ZellSafe™ Tissue Chips - **Figure 3 (a)**
- ZellScannerONE™ ChipCytometry™ instrument, Canopy Biosciences (fully integrated imaging system with HDR (32-bit)/BF Zeiss microscope and software) - **Figure 3 (b)**
- ZellExplorer App
- ZKWDataWizard application
- Fluorescence-conjugated primary antibodies (**Table 2**)

Tissue chip preparation

Tissue sections of 7-µm thickness were prepared at a standard cryostat (Leica CM1950) and mounted on treated glass coverslips (Canopy Biosciences) that were coated for better adhesion. The tissue sections were stored at -80ºC overnight to improve adhesion to the coverslip. The sections were then fixed by immersion in ice-cold 100% acetone (#9372.1, Carl Roth, Karlsruhe, Germany) for five minutes, followed by serial immersion in 90% ethanol (#5054.1, Carl Roth, Karlsruhe, Germany), 70% ethanol, and Phosphate Buffered Saline (PBS) for three minutes at 4°C, respectively. The glass coverslips with the fixed tissue samples were loaded onto ZellSafe™

Tissue Chips, chips were filled with storage buffer (Canopy Biosciences) and stored at 4 °C until, and in between, staining cycles.

Figure 3: *Chip Cytometry microfluidic "chip" and fluorescent scanning setup*

(a)

(b)

Fig 3: ZellSafe™ Chip **(a)** and fluorescent microscope plus scanning/imaging system **(b)** from Canopy Biosciences

Staining, imaging, and photobleaching

Tissue samples were taken through several rounds of iterative staining with fluorescence-conjugated antibodies. A comprehensive 26-marker antibody panel (**Table 2**) was used to target T cell populations (regulatory, effector, helper, tissue resident), other immune cells (DCs, monocytes, macrophages, NK cells), nerve structures, tissue morphology (DAPI) and HSV-1/2 pathogen, with particular focus on immune cell exhaustion (CD279, CD366, CD223, CD274) and activation markers (Ki-67, ICOS, GZMB, CD69).

Table 2: Validated Antibody Panel for Chip Cytometry Fresh Frozen Tissue Samples

	Epitope	Clone	Conjugate	Filter Set	Dilution	Company	Catalog Number	Localization
1	**CD1a**	HI149	PE	FS560	1:500	BioLegend	300105/6	Surface
	CD3	UCHT1	BUV395	FS395	1:100	BD Pharmingen	563548/6	Surface
	CD4	RPA-T4	PerCP-Cy5.5	FSPerCP	1:30	BioLegend	300529/30	Surface
	CD8a	RPA-T8	AF488	FS488	1:100	BioLegend	301024/1	Surface
2	**CD68**	KP1	AF488	FS488	1:50	SantaCruz	sc-20060 AF488	Surface
	CD303_2	AC144	PE	FS560	1:50	Miltenyi	130-113-193	Surface
3	**FOXP3**	236A/E7	PE	FS560	1:30	BD Pharmingen	560852	Intracellular
	HSV1/2	Rabbit poly	FITC	FS488	1:100	Fitzgerald	60C-CR2124RF	Surface
4	**CD279**	EH12.2H7	PE	FS560	1:30	BioLegend	329905/6	Surface
5	**Ki-67**	REA183	PE	FS560	1:30	Miltenyi	130-120-417	Intracellular
6	**CD57**	TB03	PE	FS560	1:30	Miltenyi	130-099-185	Surface
7	**CD86**	2331 (FUN-1)	PE	FS560	1:100	BD Pharmingen	560957	Surface
8	**CD69**	FN50	PE	FS560	1:30	BioLegend	310905/6	Surface
9	**CD15**	MC-480	PE	FS560	1:50	BioLegend	125605/6	Surface
10	**CD14**	HCD14	PE	FS560	1:100	BioLegend	325605/6	Surface
11	**CD45**	HI30	PE	FS560	1:100	BioLegend	304008	Surface
12	**CD123**	6H6	PE	FS560	1:100	BioLegend	306005/6	Surface
13	**CD56**	AF12-7H3	PE	FS560	1:200	Miltenyi	130-113-307	Surface
14	**CD11c**	S-HCL-3	PE	FS560	1:500	BioLegend	371503/4	Surface
15	**CD271**	ME20.4	PE	FS560	1:1000	BioLegend	345105/6	Surface
16	**GZMB**	QA16A02	PE	FS560	1:100	BioLegend	372207/8	Intracellular
	DAPI	N/A	BUV395	FS395	1:6000	Life Technologies	D3571	Intracellular
17	**CD223**	REA351	PE	FS560	1:100	Miltenyi	130-120-610	Surface
18	**CD274**	29E.2A3	PE	FS560	1:200	BioLegend	329705/6	Surface
19	**CD278**	C398.4A	PerCP-Cy5.5	FSPerCP	1:30	BioLegend	313517/8	Surface
	CD366	7D3	PE	FS560	1:30	BD Pharmingen	563422	Surface

Abbreviations: BUV = Brilliant Ultra Violet, FITC = Fluorescein isothiocyanate, AF = Alexa Fluor, PE = Phycoerythrin, PerCP = Peridinin-Chlorophyll-Protein, FS = Filter Set, GZMB = Granzyme B, CD223 = LAG-3, CD274 = PD-L1, CD279 = PD-1, CD278 = ICOS, CD366 = TIM-3

Image acquisition was performed on the ZellScannerONE™ fluorescent microscope (Canopy Biosciences). Tissue chip chambers were rinsed with wash buffer (or PBS) to remove the storage buffer before running the initial background scan. After setting the tissue geometry, an initial background scan was done in the PE channel with two seconds of photobleaching per scanned position to obtain a whole tissue image. Positions without tissue were disabled for all subsequent scans. After the initial background scan, each position with tissue was photobleached for twenty seconds and the resulting background was imaged before each cycle of staining to subtract background fluorescence. For each round of staining, antibodies were diluted in wash buffer (or PBS) to reach a working volume of 300µL. The entire diluted antibody solution was then pipetted into the chip chamber and incubated in the dark at room temperature for fifteen minutes. After antibody incubation, the chip chamber was washed thoroughly with 10mL wash buffer before imaging. Images were acquired in the necessary fluorescent channels and the cycle was repeated until all biomarkers have been stained and imaged. The images obtained were examined using ZellExplorer data analysis software (Canopy Biosciences). Net-fluorescence images were created by deducting autofluorescence from the fluorescence image of each cycle and position.

Images were reviewed and adjustments were made to the dynamic compression and background factor, if necessary. Fluorescent images were exported as 8-bit .png files, as whole stitched images, single position tiles, and strips. While it is unnecessary to export the background scan images for each of the markers, it is helpful to have at least one background image per sample to use for normalizing tissue size across samples for data analysis.

Data analysis

Data analysis was performed by a combination of ImageJ/Fiji (for cleaning, splitting, and merging images), Python (for stitching image “tiles”, or positions, together into a whole tissue image), and Cellpose 2.0 (for automated quantification of phenotypically distinct cell populations within our tissue samples).

Software:

- Cellpose 2.0
- ImageJ/Fiji
- GraphPad Prism 9

ImageJ/Fiji:

ImageJ/Fiji, a biological image analysis application, was used for preprocessing our fluorescent images prior to automated cell segmentation. These tools offer a wide array of biological image analysis features, fostering collaboration between computer scientists and biologists through customizable macros and plugins [49], [51]. Multicolor images were loaded into ImageJ/Fiji, "cleaned" as necessary, and split into single color channels and saved as grayscale versions. Image cleaning aims to mask over artificial signals, such as bright 'blobs' caused by debris or autofluorescence. We used the built-in channel merger function to create composite images of up to seven markers. Cell counts (produced by automated cell segmentation described in the following section) were normalized across tissue samples of varying sizes to get the number of cells per square millimeter (mm^2). Normalization of tissue size was done in ImageJ using the polygon tool to trace the tissue perimeter, then setting the scale to two pixels/micron (distance in pixels = 1, known distance = 0.5, pixel aspect ratio = 1, unit of length = microns, and apply globally). The resulting area measurement was given in microns and was then translated to mm^2 units.

Cellpose:

Cellpose model cytotrain7 (cyto7), the latest iteration of our model in Cellpose, was used for cell segmentation. Cyto7's performance results from the 7 ground truth training sessions fed back into the system The performance of cyto7 results from the 7 ground truth training sessions that were fed back into the system, using the human-in-the-loop approach of Cellpose 2.0. Specific parameters were optimized for our samples and set as defaults.

The tuning parameters used in our segmentation include:

(1) Average intensity
(2) Cell diameter
(3) Minimum size
(4) Flow threshold
(5) Total minimum intensity
(6) Cell probability
(7) Resampling

These parameters were optimized for our skin tissue samples, and the only ones that needed further tuning were average intensity, minimum size, and flow threshold. For CD3 segmentation, we changed the average intensity to 20, the minimum size to 100, and the flow to 0.5. For CD4 segmentation, we changed average intensity to 10, min size to 100, the average intensity to 10, min size to 100, and flow to 0.5. For CD8 segmentation, we changed average intensity to 20, min size to 100, the average intensity to 20, min size to 100, and flow to 0.5. After that, we retrieved the mask files and did a mask-mask cell phenotyping analysis at 0.6 overlap threshold to get the four CD3, CD4, CD8 populations. These four populations include: CD3+CD4+CD8+ (double positive, DP), CD3+CD4+CD8- (CD4+ T cells), CD3+CD4-CD8+ (CD8+ T cells), and CD3+CD4-CD8- (double negative, DN). These four main T cell subpopulations are then included in the co-expression analysis with other markers of interest from our list of exhaustion and activation-associated markers. The T cell populations obtained (CD3+CD4+CD8- and CD3+CD4-CD8+) were used for co-expression analysis with other markers via their intensities. The intensities of the different markers within the T cells identified were the tuning parameters used to determine the positivity or negativity of these additional markers within the T cell population. There are three ways to measure intensity: total, mean, and median. For this analysis, we used total intensity.

Chapter 6 – Results & Discussion

T cells infiltrate lesion tissue to control HSV reactivation

As expected from previous studies [65], [66], [67], we observed massive infiltration of immune cells, the majority being T cells, in recently healed lesions. The density of T cells decreased dramatically by the 8 weeks post-healed (8wph) biopsy for all subjects.

Figure 4(a) shows the averaged T cell densities (CD3+ cells per mm^2 of tissue area) for the four subjects included in this study, at the newly healed lesion biopsy and at 8wph. Although the difference between T cell density during lesion compared to 8wph is not statistically significant, figures **4(d)** and **4(e)** exemplify the fold decrease difference in T cell density between healed and post-healed skin for each subject individually. Figures **4(b)** and **4(c)** show the averaged CD8+ and CD4+ T cell densities, respectively, from Healed to Post-Healed. The averaged CD4+ T cell densities at Healed and Post-Healed were statistically significant with a p-value of .0474.

Subject A had a much lower cell density to at the healed timepoint compared to B, C, and D, and therefore, it is challenging to see the change in infiltrating immune cells from healed to post-healed. **Table 3** shows the fold decrease in T cell density from healed to post-healed for all subjects individually. Subjects C and D experienced the largest decrease in T cell density, and notably, they are also the subjects with the highest HSV shedding rates, signifying the least amount of control over HSV infection.

Figure 4: *Average T cell densities over the course of lesion healing*

(a)

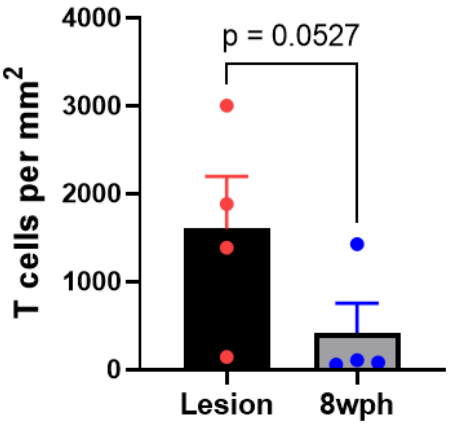

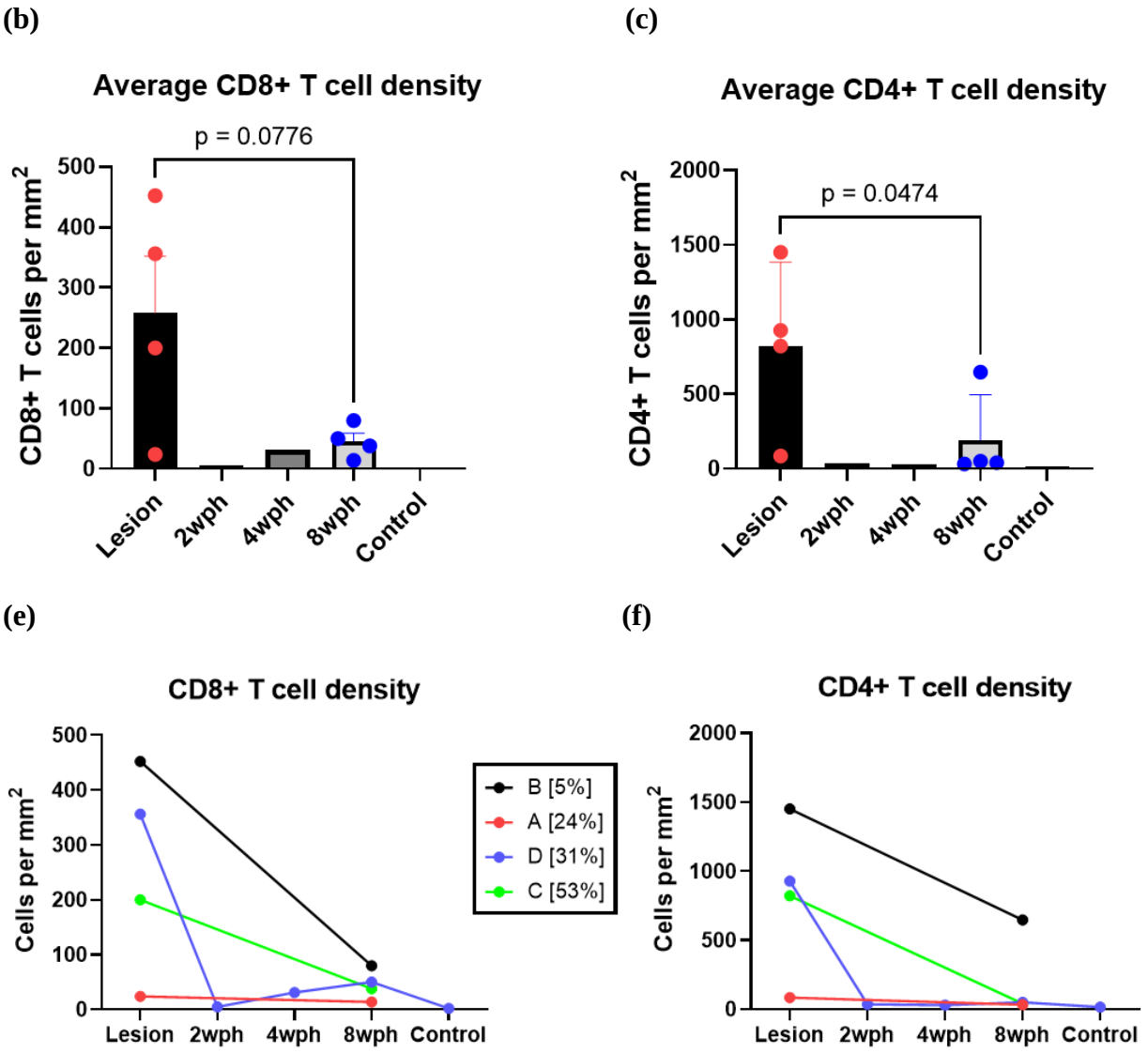

Fig 4: (a) T cells per mm^2 averaged for all subjects at healed lesion timepoint and 8-weeks post healed timepoint. SEM bars shown, paired t-test was performed, with a non-significant p-value of .0527. **(b)** CD8+ T cells per mm^2 averaged for all subjects at healed lesion timepoint and 8-weeks post healed timepoint. SEM bars shown, paired t-test was performed, with a non-significant p-value of .0776. **(c)** CD4+ T cells per mm^2 averaged for all subjects at healed lesion timepoint and 8-weeks post healed timepoint. SEM bars shown, paired t-test was performed, with a significant p-value of .0474. CD8+ T cell density **(e)** and CD4+ T cell density **(f)** over lesion healing for all subjects, with their respective HSV shedding rates shown in parentheses.

Table 3: *Decreases in T cell density over lesion healing*

Subject	% HSV shedding	CD8+ T cells per mm^2	CD4+ T cells per mm^2	CD3+ T cells per mm^2
B	5%	**-5.7 fold**	**-2.2 fold**	**-2.1 fold**
A	24%	**-1.7 fold**	**-2.6 fold**	**-2.6 fold**
D	31%	**-7.1 fold**	**-18.6 fold**	**-22.7 fold**
C	52%	**-5.3 fold**	**-20 fold**	**-12.9 fold**

Table 3: Fold decrease (bolded) in T cell density (cells per mm^2) from Healed to Post-Healed (8wph) for CD4+ T cells, CD8+ T cells, and T cells in general (CD3+). Fold decrease was determined by dividing the Healed cells/mm^2 by Post-Healed cells/mm^2.

There were changes to T cell composition throughout the lesion healing process for each subject. Figure 5 shows the percentage out of all CD3+ cells that also express CD4, CD8, both, or neither. Subjects A and C experienced an expansion in the proportion CD8+ T cells from Healed (Les) to Post-Healed (8wph). Subject D showed an increased population of CD4+ T cells across healing timepoints, with a decrease in CD8+ T cells. Subject B showed a differing trend from the rest, with a decrease in the percentage of CD8+ and CD4+ T cells at Post-Healed timepoint, but an increase in the percentage of Double Positive (DP). However, the DP and DN population proportions are likely overexaggerated due to staining and imaging issues with CD4 (contributing to DN) and signal spillover from nearby cells (contributing to DP). These populations were investigated by visual inspection of images with the Cellpose masks overlayed to assess accuracy.

Figure 5: *T cell composition across subjects and lesion healing*

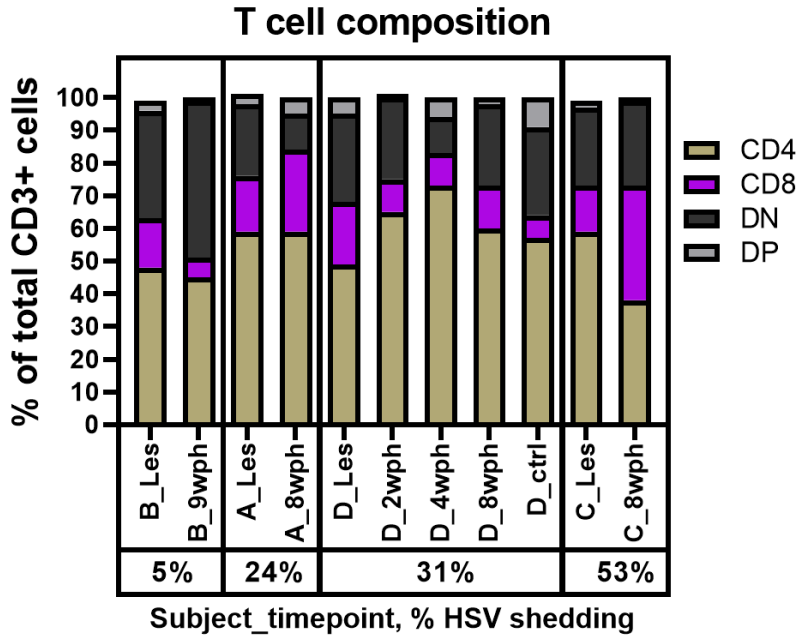

Fig 5: T cell composition (CD3+CD4+, CD3+CD8+, CD3+CD8-CD4- double negative DN, and CD3+CD8+CD4+ double positive DP) across subjects and lesion healing. Percent HSV shedding rate for each subject is shown at bottom of the x axis.

Activation marker expression is usually higher in healed tissue than in post-healed tissue

Here, we used CD69 as a marker for early activation by taking the percent of CD69+ cells minus the percent of CD69+PD-1+ cells to get the resulting CD69+PD-1- activated cells. GZMB expression stayed low (less than 10%) for all subjects. This is likely due to the extracellular expression of GZMB observed across all subject samples and healing timepoints. GZMB marker positivity was counted when there was overlap between the GZMB signal and the T cell markers. However, in many samples, GZMB did not overlap with any cells and therefore was not counted. CD69 and ICOS tended to be the most highly expressed markers found in newly healed lesion tissue, whereas GZMB and Ki-67 were expressed at lower levels. Samples from subjects B and D showed decreased expression of all activation markers. For Subject D, expression of CD69+PD-1- started to increase again at 4wph and 8wph, which could result from asymptomatic shedding. Expression levels for Subject A decreased across healing except for CD69, which increased at 8wph. The same pattern observed with Subject A was seen with Subject C.

Figure 6: *Identification of activated CD8⁺ T cell in healed lesion tissue*

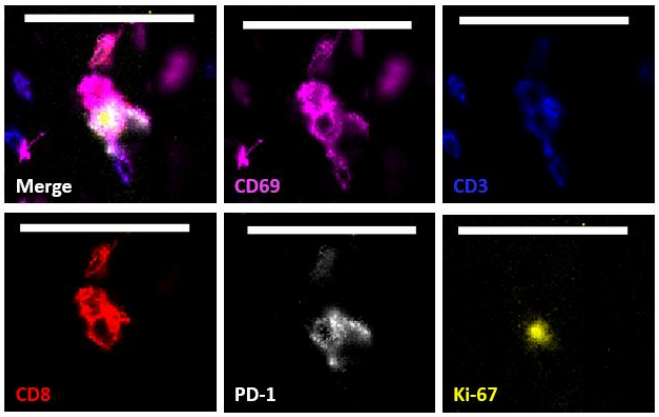

Fig 6: An activated CD8+ T cell is identified via a combination of various markers. All markers are merged together in the top left image and individual markers are shown in the other five images, scale bar = 50µm. The combination of Ki-67 (proliferation) with CD69 (early activation) leads us to believe this cell is in an activated state. Additionally, PD-1 can be transiently expressed for a short period of time following activation.

Figure 7: *Individual activation markers across healing*

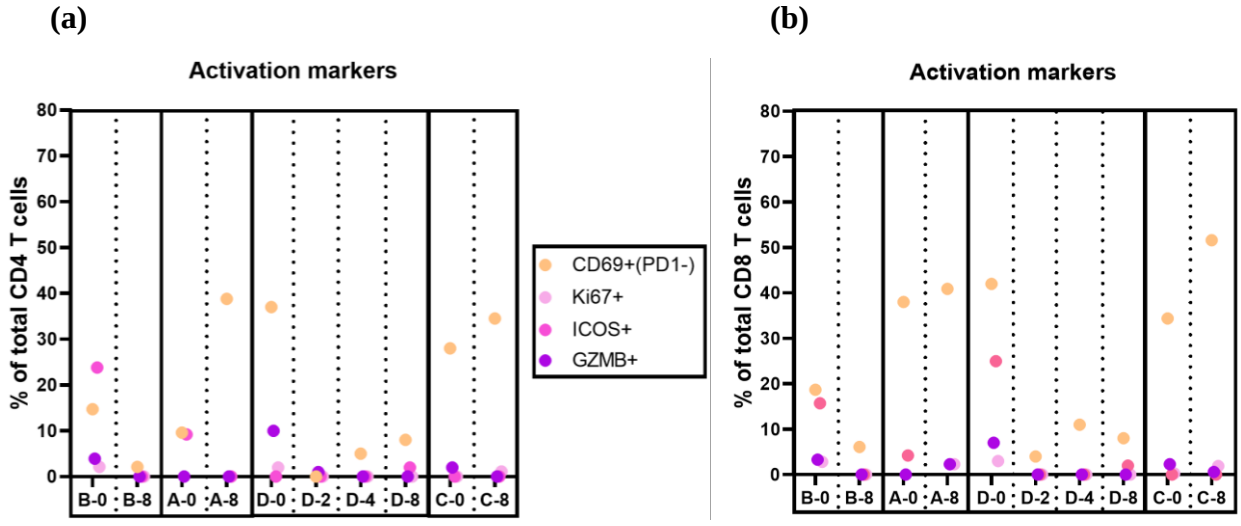

Fig 7: Activation markers found on CD4+ T cells **(a)** and CD8+ T cells **(b)** across healing (naming: D-0 = Subject D biopsy taken at 0-weeks post healed, or "lesion")

Exhaustion marker expression varied across subjects and lesion healing timepoints

CD69+PD-1+ is a marker combination for tissue residency, which is included in this section alongside exhaustion markers and is represented as a green triangle. As cells transition from an activated state to exhausted, their expression of CD69 generally decreases and expression of PD-1 increases. Here, we calculated PD-1+CD69- by taking the percent of PD-1+ cells minus percent of PD-1+CD69+ cells. Looking at the expression of inhibitory receptors (PD-1, TIM-3, and LAG-3) over the course of lesion healing, it is harder to distinguish a universal trend than in the activation marker expression in the previous section. Subject A shows decreased expression of inhibitory receptors over time. The same is true for Subject B, except the dramatic increase in LAG-3 expression on CD8+ T cells at 8wph. Subject D has moderate expression of all three inhibitory receptors in the healed lesion tissue, then experiences a spike in PD-1+CD69- at 2wph which steadily decreases at 4wph and 8wph. Subject C shows comparable levels of the inhibitory receptors, with TIM-3 expression the highest.

Figure 8: *Identification of exhausted CD4^{+} T cell with multiple inhibitory receptors (IRs)*

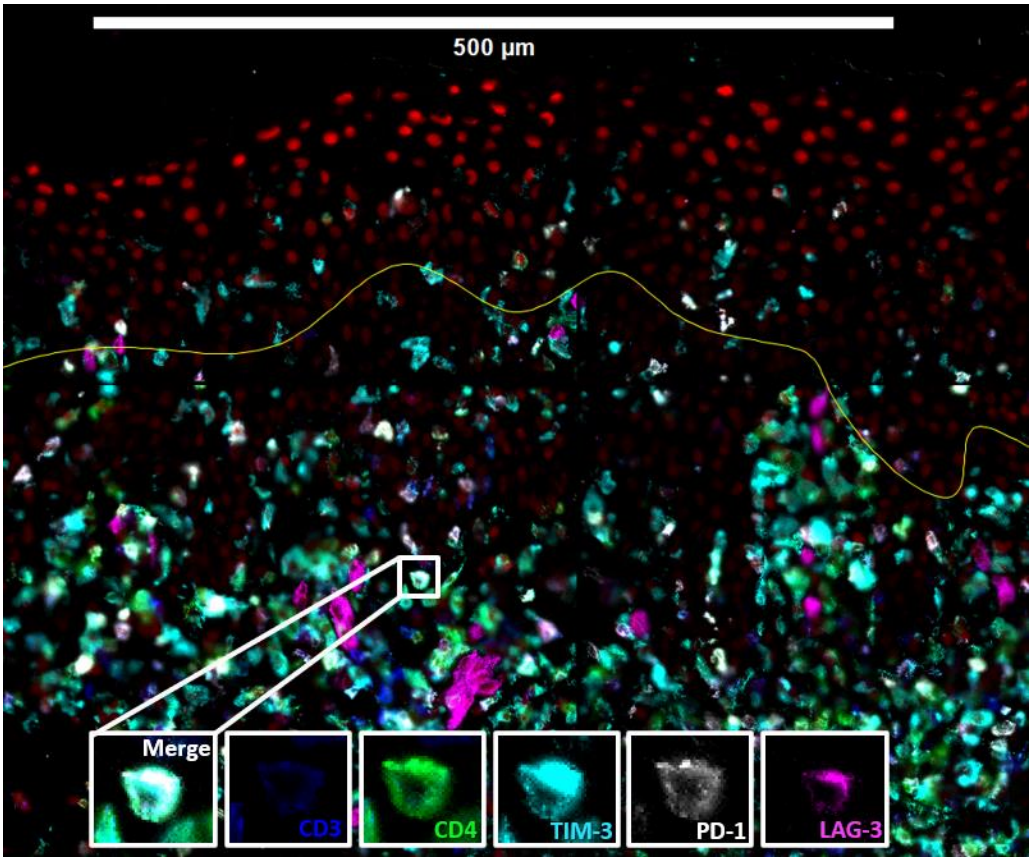

Fig 8: This image is of Subject D healed lesion tissue, zoomed into a cell near the DEJ, in the upper dermis. This cell is positive for CD3 and CD4, making it a CD4+ T cell. Additionally, this T cell expresses TIM-3, PD-1, and LAG-3, each of which are inhibitory receptors. As mentioned, categorization of a cell as exhausted is more definitive the more inhibitory receptors are detected on the cell. In this figure the DEJ is traced in yellow and DAPI staining is shown in red.

Figure 9: *Individual exhaustion markers across healing*

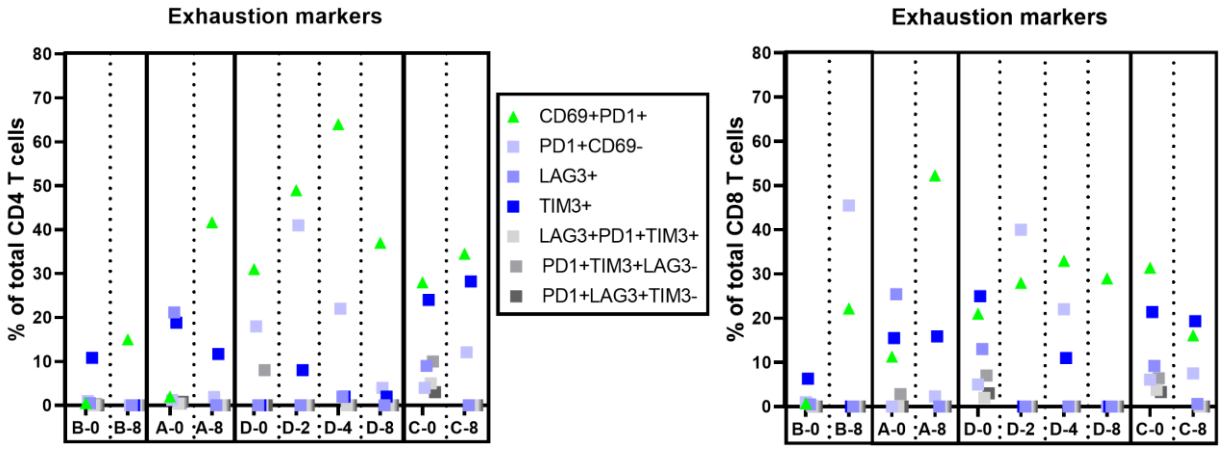

Fig 9: Exhaustion markers found on CD4+ T cells **(a)** and CD8+ T cells **(b)** across healing (naming convention: D-0 = Subject D biopsy taken at 0-weeks post healed, or "lesion" timepoint)

Regulatory T cells

It is likely that Tregs can contribute to T cell exhaustion due to their immunoregulatory function [34]. Reduction of Tregs plus blockade of PD-1+ was shown to have a synergistic positive effect on reversing T cell exhaustion and controlling viral load [46]. This section includes in-depth characterization of conventional Tregs (CD4+FoxP3+) and CD3+CD8+ Tregs.

Figure 10: *Visualization of $CD8^+$ Tregs in tissue*

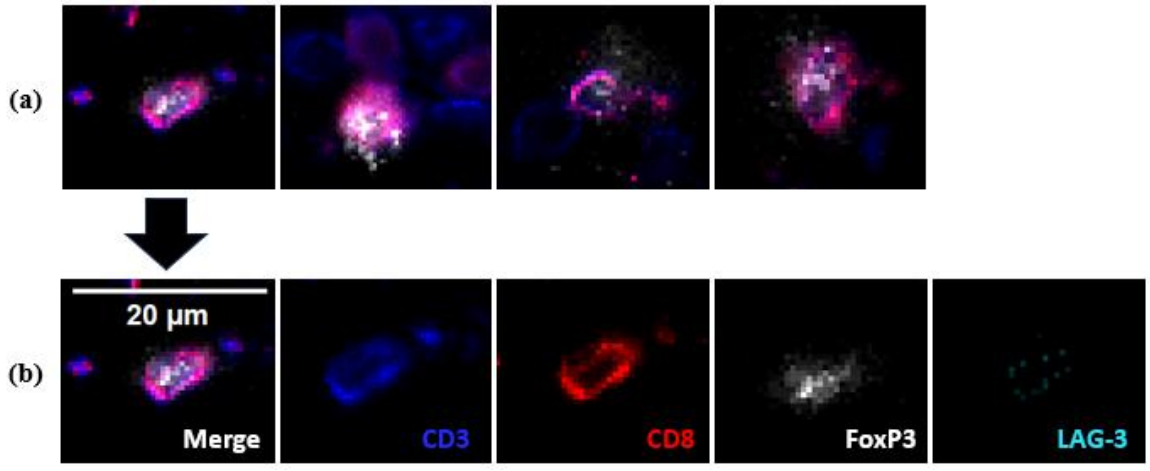

Fig 10: Four CD8+ Tregs **(a)** found in Subject C healed lesion biopsy. Foxp3 in white, CD8 in red, and CD3 in blue. Figure 11 **(b)** shows all markers separately for one of Tregs which expressed a faint amount of LAG-3, shown in cyan.

In **Figure 11**, we investigate the percentage of Tregs found at different timepoints across lesion healing. **Table 4** shows the percent HSV shedding and the percent of CD4+ Tregs for each subject and timepoint. Subjects D and C (highest shedders) had a higher percentage of CD4+ Tregs compared to Subject B (lowest shedder). The percentage of CD4+ Tregs out of all CD4+ T cells found in biopsies increased for subjects B (0.2% to 4.6%) and C (5% to 13%), but slightly decreased for Subject D (from 15.8% to 13%). A higher number of Tregs present in newly healed lesion tissue is associated with higher viral replication. Since CD8+ Tregs are a rarer subset than conventional CD4+ Tregs, the percentage of these remained close to baseline in all timepoints and patients.

Figure 12 shows Treg density over lesion healing, for CD8+ and CD4+ Tregs. The number of CD4+ Tregs per mm^2 increased from healed to post-healed for Subject B, but decreased for subjects D and C. Once again, CD8+ Tregs remained at a low level across healing without remarkable changes. Subject D had the highest density of CD4+ Tregs at the healed lesion timepoint with 146 cells per mm^2.

Figure 13 shows a multiplexed image from Subject D's healed lesion, which had the highest CD4+ Treg density. In this tissue, we were able to identify a proliferating CD4+ Treg located in the upper dermis, near the DEJ. The local abundance of Treg cells within the tissue at the site could elucidate the sustained presence of CD4+ Tregs across the lesion, post-recovery period, and in the unaffected tissue of Subject D. This discovery suggests that the tissue microenvironment may stimulate Treg cell proliferation. Tregs are vital for immune regulation, preserving tolerance, and curtailing excessive immune reactions. The identification of proliferating Tregs in the skin suggests their contribution to immune balance and tolerance mechanisms.

Figures 14 and 15 show an in-depth characterization of CD4+ Tregs and CD8+ Tregs, respectively, found in healed lesion tissue from Subject C.

Figure 16 illustrates the identification of a CD8+ Tissue-Resident Memory (TRM) T cell through the analysis of markers expressed on its cell surface. This observation is evident in the healed lesion tissue of Subject D.

Figure 17 illustrates a transition in the functional status of T cells, moving from activation to tissue residency (survival). This functional transformation occurs from the phase of healing to the post-healing stage. This pattern was observed across all subjects, with the exception of Subject C, who exhibited the highest rate of HSV shedding, indicating the least control over HSV infection.

Figure 11: *Percent of $CD4^+$ and $CD8^+$ Tregs found in skin throughout healing*

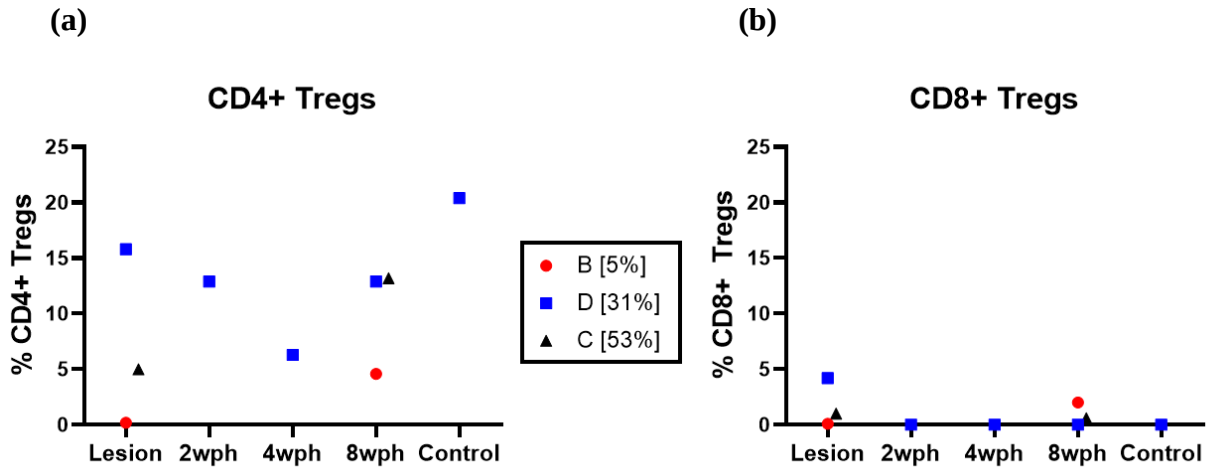

Fig 11: Percent of CD4+ Tregs out of all CD4+ T cells **(a)** across lesion healing for Subjects B, C, and D. Percent of CD8+ Tregs out of all CD8+ T cells **(b)** is shown on the right. In the key, HSV shedding rate is shown next to the Subject ID. Note that Subject A is not included because FoxP3 staining was unsuccessful for that sample.

Table 4: *Percent $CD4^+$ Tregs present in tissue, with subject HSV shedding rate*

Subject ID	**A**	**B**	**C**	**D**
HSV shedding rate	**24%**	**5%**	**53%**	**31%**
Lesion	N/A	0.2%	5%	15.8%
2wph	N/A	N/A	N/A	13%
4wph	N/A	N/A	N/A	6.3%
8wph	N/A	4.6%	13%	13%
Control	N/A	N/A	N/A	20.4%

Table 4: This table shows the percentage of CD4+ Treg cells (CD3+CD4+FoxP3+) out of all CD4+ T cells (CD3+CD4+) over lesion healing for each subject, along with their HSV shedding rate. FoxP3 staining was unsuccessful for Subject A's biopsy samples, and thus are not included in subsequent regulatory T cell analyses.

Figure 12: *Density of $CD4^+$ and $CD8^+$ Tregs across healing*

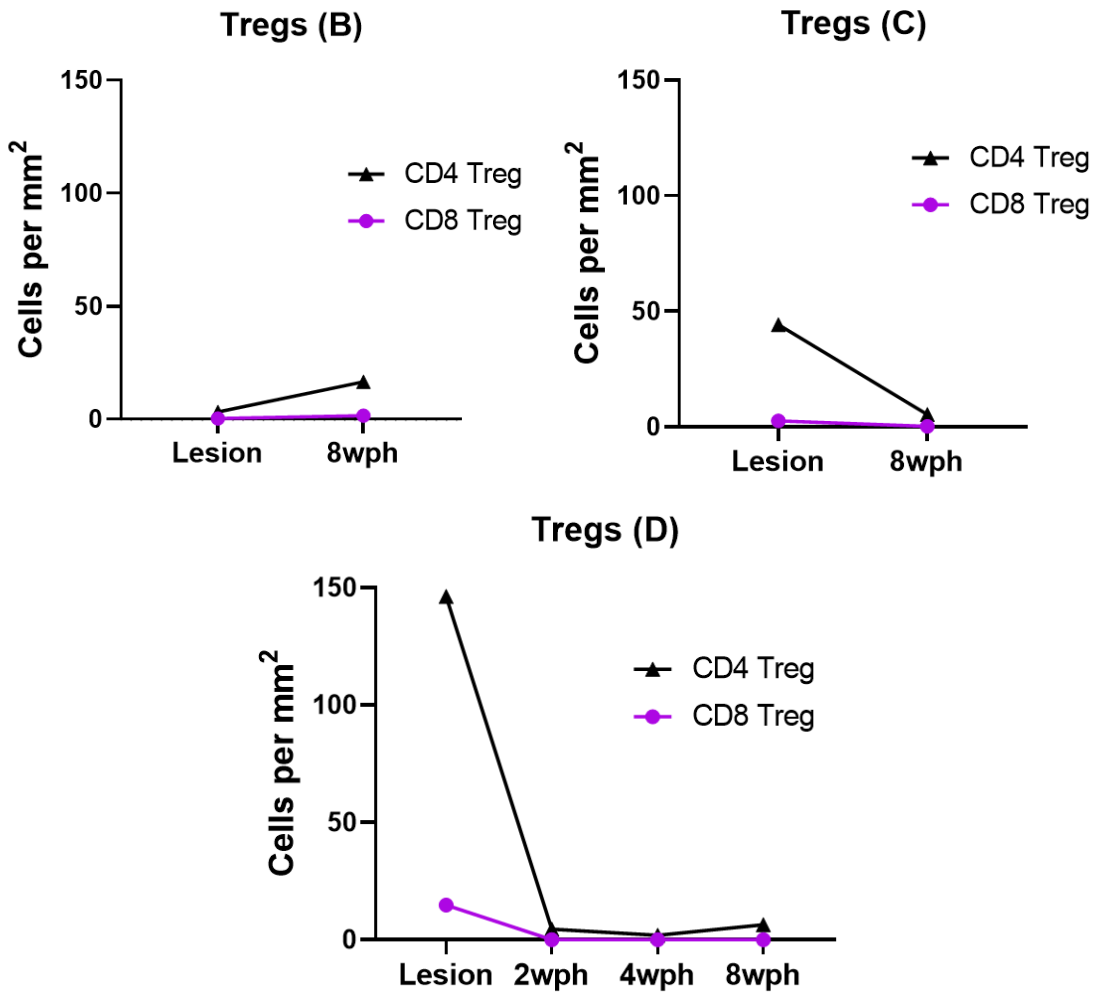

Fig 12: Line graph comparison of CD4+ and CD8+ Tregs over lesion healing as determined by Cellpose counts for cells expressing marker combinations of CD3+CD4+FoxP3+ or CD3+CD8+FoxP3+. CD4+ Treg (black, triangle) and CD8+ Treg (purple, circle) density across lesion healing for Subjects B, C, and D shown in cells per mm^2.

Figure 13: *Identification of proliferating CD4^{+} Treg near the DEJ of newly healed lesion skin*

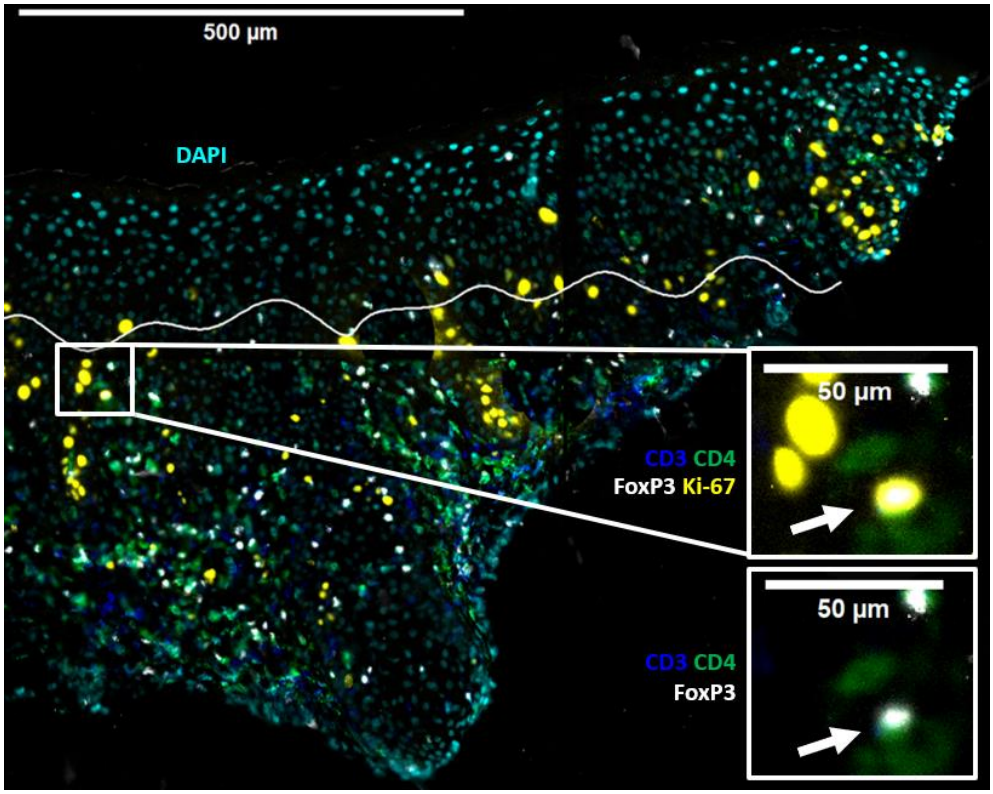

Fig 13: Identification of proliferating CD4+ Treg near the DEJ. The DEJ traced with a white line and DAPI (cyan) staining is shown for easier visualization of tissue morphology. Scale bar = 500µm. Magnified sections shows all markers with and without Ki-67. Ki-67 indicates proliferation and is shown in yellow. Scale bar for magnified sections = 50µm.

Figure 14: *Characterization of CD4^{+} Tregs in newly healed lesion biopsy*

(a) Distribution of CD4+ Tregs throughout healed lesion tissue

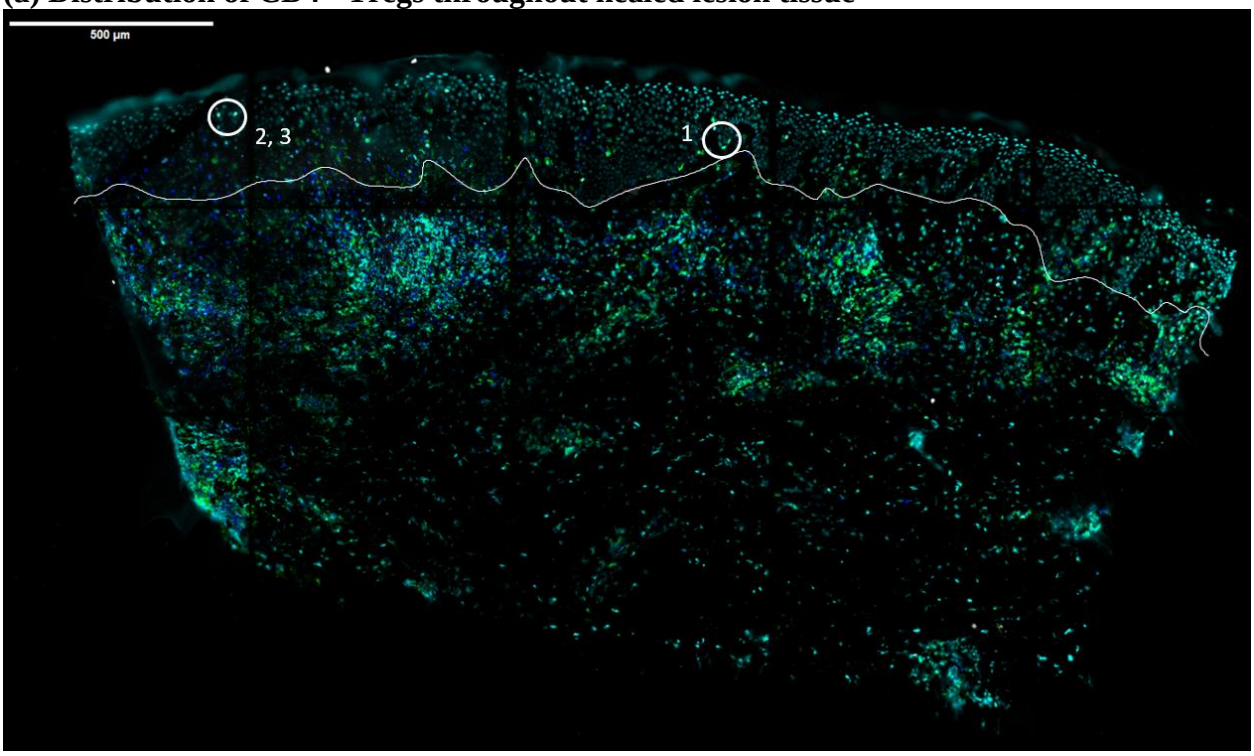

(b) Characterization of Treg #1

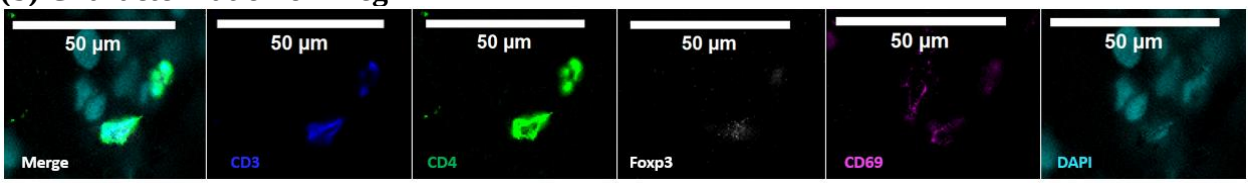

(c) Characterization of Tregs #2 and #3

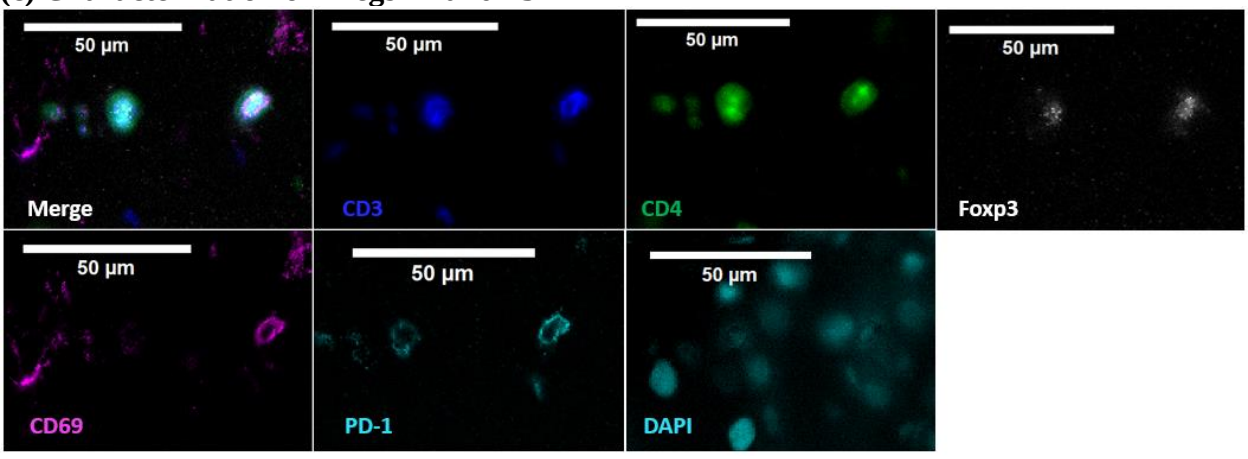

Fig 14: (a) Subject C, CD4+ Treg distribution throughout healed lesion tissue, indicated by white circles. DEJ is traced with a white line; the section above the DEJ is the epidermis and the section below it is the dermis. All of these Tregs are located in the epidermis, near the DEJ. DAPI staining is shown in cyan to highlight tissue morphology. Scale bar = 500µm. **(b) CD4+**

Treg #1 characterization: Treg #1 was negative for PD-1, GZMB, and Ki-67 and positive for all markers shown (FoxP3, CD69, CD4, CD3). From this combination of markers, we can assume that Treg #1 is a newly activated CD4+ Treg because it is CD69+ but PD-1-. **(c) CD4+ Treg #2 and #3 characterization:** Tregs #2 and #3 were shown together due to their closeness in the tissue. Both of these CD4+ Tregs were negative for GZMB and Ki-67 but positive for all markers illustrated (CD3, CD4, FoxP3, CD69, and PD-1). Tregs 2 and 3 are likely Tissue Resident Memory Tregs because they co-expressed CD69 and PD-1.

Figure 15: *Characterization of $CD8^+$ Tregs in newly healed lesion biopsy*

(a) Distribution of CD8+ Tregs throughout healed lesion tissue

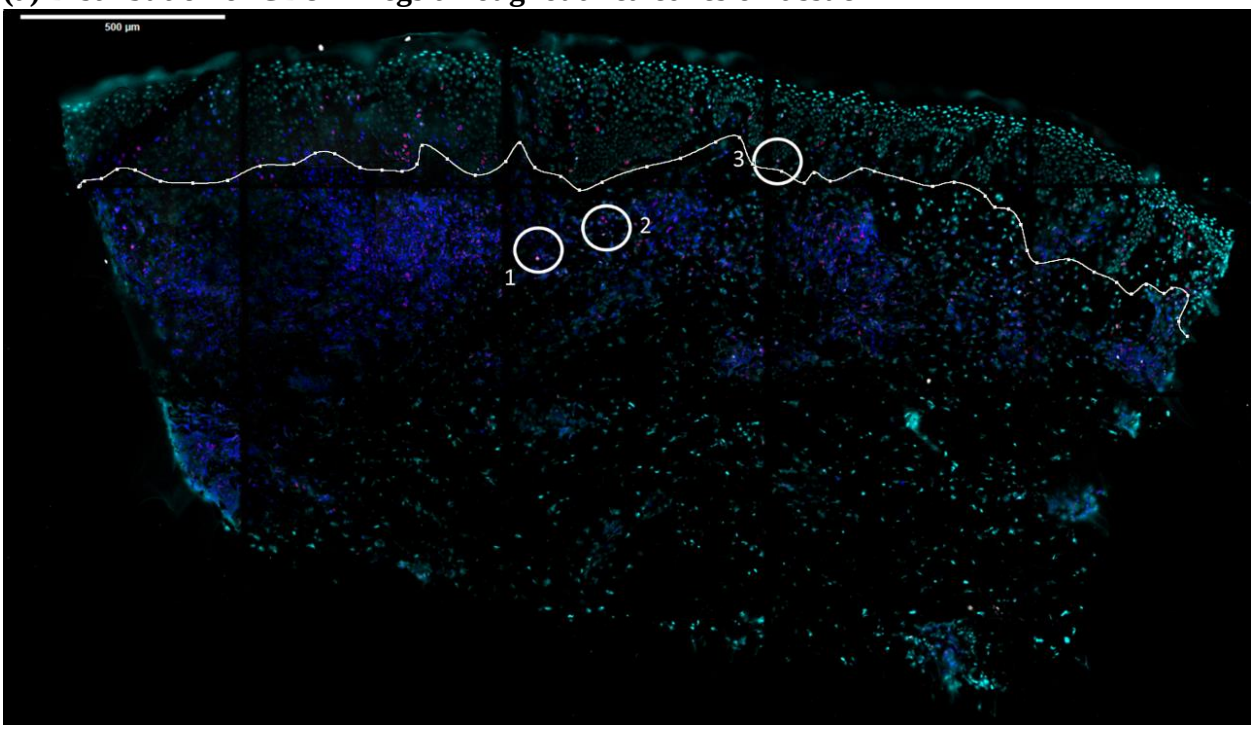

(b) Characterization of Treg #1

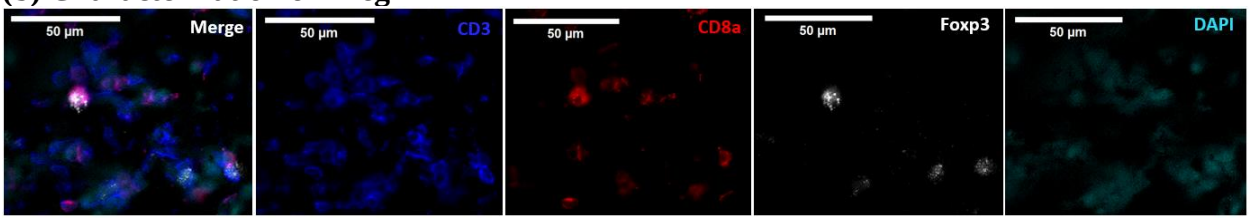

(c) Characterization of Treg #2

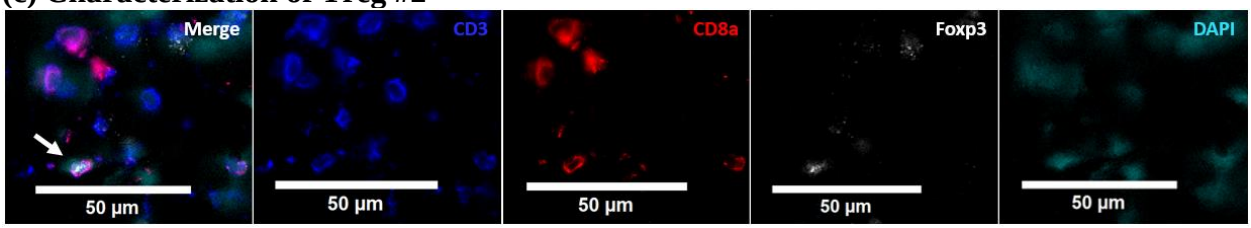

(d) Characterization of Treg #3

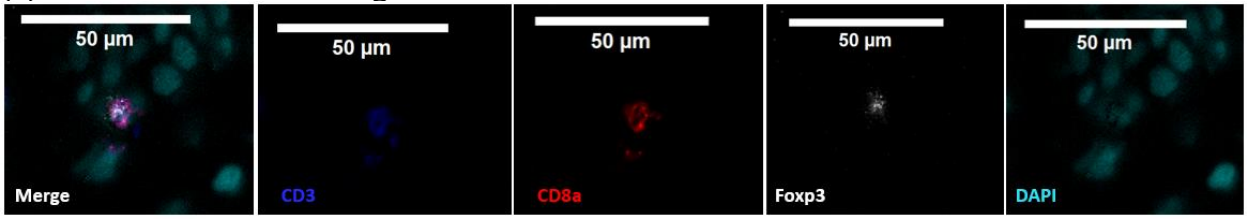

Fig 15: (a) Subject C, CD8+ Treg distribution throughout healed lesion tissue, indicated by white circles. DEJ is traced with a white line; the section above the DEJ is the epidermis and the section below it is the dermis. Scale bar = 500µm. Tregs 1 and 2 are in the dermis and Treg 3 is close to the DEJ. DAPI is depicted in cyan to enhance the visualization of tissue structure. **(b) CD8+ Treg #1 characterization:** CD8+ Treg #1 is shown up close with all positive markers (CD3, CD8, FoxP3). Treg #1 was negative for PD-1, Ki-67, and CD69. Due to the marker expression, we can infer that this Treg is a CD8+ Treg without a specific tissue residency, exhaustion, or activation profile. **(c) CD8+ Treg #2 characterization:** CD8+ Treg #2 expressed PD-1 and CD69 but not Ki-67, indicating it as a tissue resident memory Treg without proliferation. **(d) CD8+ Treg #3 characterization:** CD8+ Treg #3 expressed CD69 but lacked PD-1 or Ki-67, indicating it is likely a recently activated CD8+ Treg.

T cell functional states shift from activation to survival over course of lesion healing

Figure 16: *Identification of CD8^{+} TRM cell near DEJ in healed lesion biopsy*

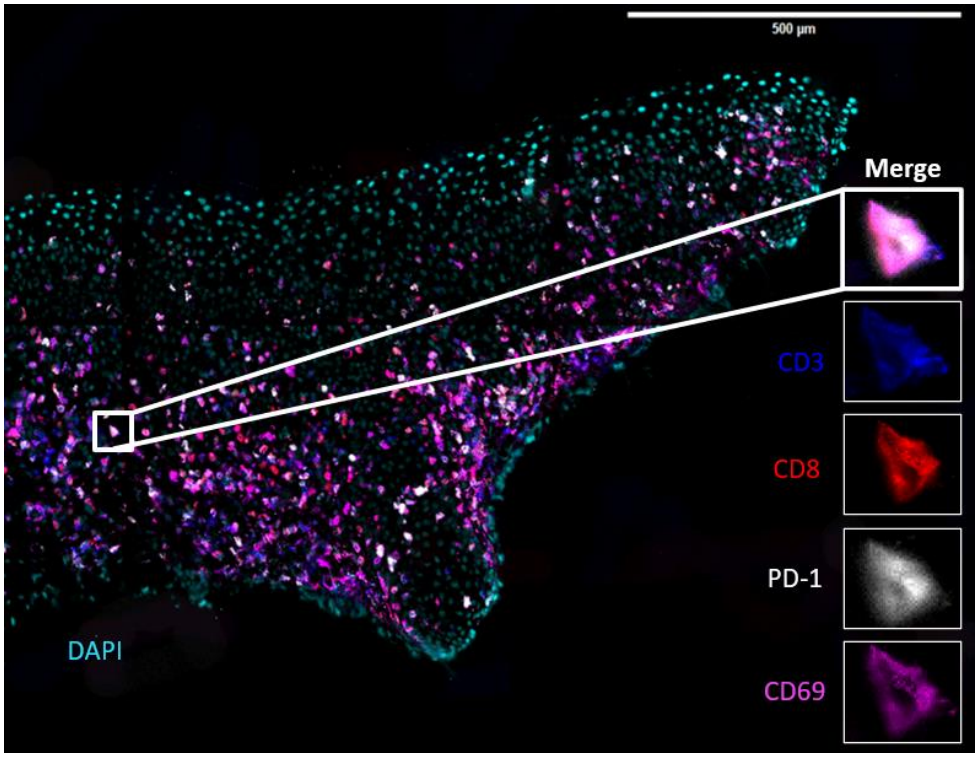

Fig 16: Identification of CD8+ TRM cell based off marker combinations, specifically CD69+PD-1+ phenotype. This image is the upper right side of Subject D healed lesion tissue, zoomed in on a single cell near the DEJ. The cell is positive for CD3, CD8, PD-1, and CD69. CD3 plus CD8 identifies CD8+ T cells. Since CD69 is co-expressed with PD-1, we can conclude that the function of CD69 here is tissue residency. Scale bar = 500µm.

Figure 17: *Shift from CD69^{+}PD-1^{-} (activation) to CD69^{+}PD-1^{+} (tissue residency)*

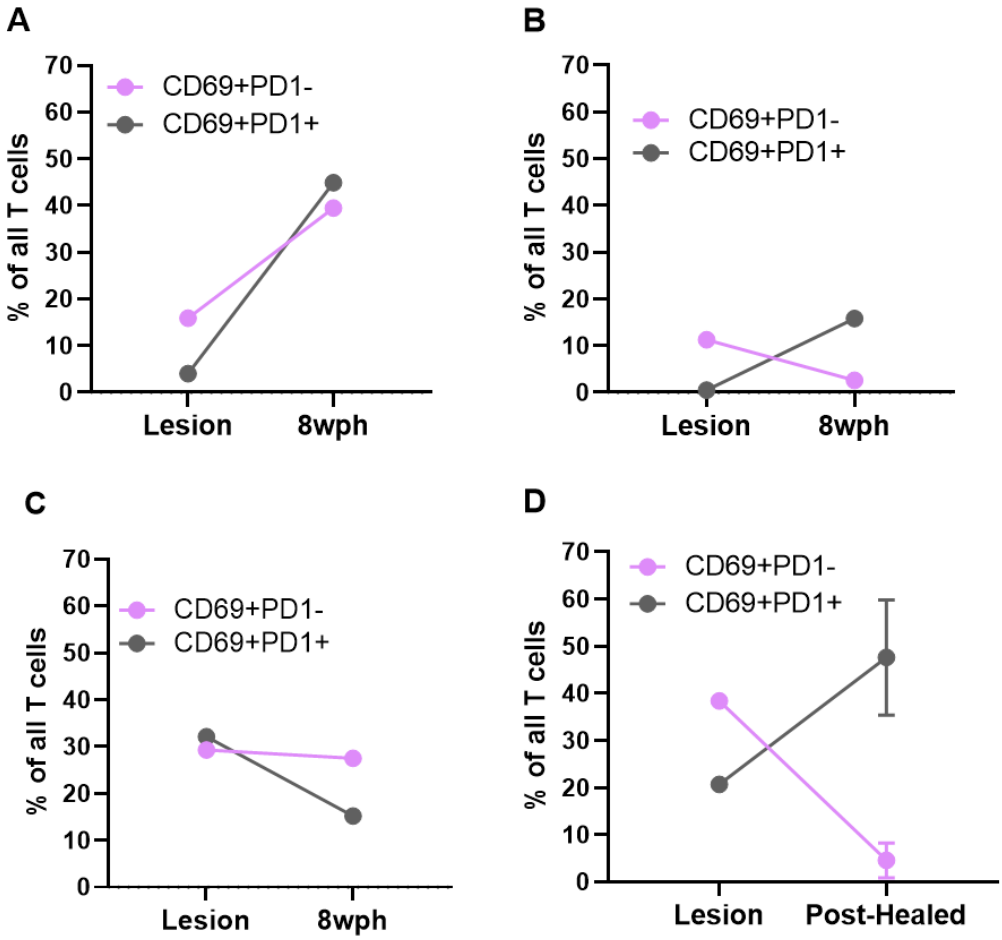

Fig 17: The percent of all T cells (CD3+ cells) expressing either CD69+PD-1- (activation phenotype) or CD69+PD-1+ (tissue-resident memory, TRM, phenotype) for all subjects A through D at biopsy timepoints of newly healed lesion and 8-weeks post healed. For Subject D, the post-healed timepoints (2wph, 4wph, and 8wph) were averaged and the SEM bars are shown. Subjects A, B, and D showed a shift in the dominant population phenotype from activation to tissue residency from healed to post-healed. Subject C, who had the highest rate of HSV shedding at 53%, experienced the opposite trend, shifting the dominant population from tissue residency to activation.

Chapter 7 – Conclusion

Summary of findings

T cell density & composition

T cell density (cells per mm^2) peaks during the healed lesion timepoint and drops dramatically in the post-healed timepoints. This phenomenon is observed across all T cell subsets, including CD3+, CD4+, and CD8+ T cells

T cell composition (proportion of CD4+, CD8+, double negative DN, and double positive DP T cells) varies slightly between subjects and across lesion healing. However, no obvious trends were observed in the changes to T cell composition.

Double negative (DN) T cells are a rare subset of peripheral T cells that express CD3 but are negative for both CD4 and CD8 [61]. 3-5% of T cells in peripheral blood are DN T cells [61]. These cells can have both innate and adaptive immune properties and their function varies depending on environment [61]. Our segmentation counts showed levels of DN T cells that were higher than the average 3-5% found in blood, and ours were also detected in tissue. We believe the reason behind the higher than expected levels of DN T cells detected in tissue reflect a staining/imaging issue with the CD4 antibody conjugate used in this project. The high DN T cell counts likely are a product of CD4 staining as it was randomly blurry in some regions, resulting in missed detection by the segmentation algorithm.

We also observed higher than expected levels of double positive (DP) T cells. This is likely a result of signal spillover between closely packed cells, especially at the lesion timepoint when T cell density is highest.

T cell activation markers

Percent and density of T cell activation markers, including Ki-67, CD69+PD-1-, GZMB, and ICOS, tended to decrease over the course of lesion healing. The exception to this trend was Subject A which showed comparable levels of CD69+PD-1- at both lesion and 8-weeks post healed timepoints. However, ICOS expression for Subject A decreased from lesion to 8-weeks post healed. There was no Ki-67 or GZMB expression for Subject A. It is worth noting that Subject A had the lowest density of T cells compared to the three other subject samples.

T cell exhaustion markers

Percent and density of T cell exhaustion markers (or inhibitory receptors), including PD-1, TIM-3, and LAG-3, showed varying expression trends across healing and between subject samples. Subject D (31% HSV shedding) had the highest expression of all three inhibitory receptors at the healed lesion timepoint and virtually no expression from 2wph to 8wph and 8w control for both CD4+ and CD8+ T cells. Subject A (24% HSV shedding) had low level expression of inhibitory receptors in both CD4+ and CD8+ T cells and at healed lesion and 8wph. Subject C (53% HSV shedding) had high expression of all three inhibitory receptors at the healed lesion timepoint and markedly decreased expression at 8wph, for both CD4+ and CD8+ T cells.. In Subject B (5% HSV shedding), elevated levels of TIM-3 were observed at the healed lesion in both CD4+ and CD8+ T cells. This expression profile transitioned to a predominance of PD-1+CD69- T cells at 8 weeks post-healed.

Regulation

Regulatory T cells were distributed throughout the dermal and, in some cases, the epidermal tissue. In most cases, the percentage of Tregs present in the skin increased from the healed to post-healed lesion tissue. The density of conventional Tregs decreased from the healed to post-healed stage in subjects C and D, whereas it exhibited a slight increase in subject B. Interestingly, subjects with highest viral shedding rates, C (53%) and D (31%), have high Treg presence during lesion (5.8% and 15%, respectively) and post healing (13% and 13%), compared to subject B (5%), who had the least amount of HSV shedding, also had lowest frequency (0.2% for lesion and 5% for 8wph). Although small in sample size, our data might suggest a positive correlative relationship between Treg and HSV disease. High frequency of CD4+ Treg might be associated with a high HSV shedding rate in skin tissue. Future studies are needed to further test this hypothesis.

Survival

In terms of tissue residency, or survival, we observed a population shift from the majority of T cells expressing CD69+PD-1- as an activation phenotype during the healed timepoint to the majority of T cells expressing CD69+PD-1+ as a marker of cell survival in the post-healed

phase. T cells expressing this survival phenotype are likely to be Tissue Resident Memory T cells, which are imperative for controlling subsequent HSV reactivations.

Differences related to HSV shedding rate

The subject with the highest HSV shedding rate, and subsequently, least control over HSV infection, was Subject C at 53% shedding rate. In terms of the ratio of activated and survival functional state T cells, Subject C was the only one that experienced a decrease in tissue residency phenotype and increase in activation phenotype across healing. This makes sense because TRM cells are associated with quicker and more effective control of localized reactivating infection.

Challenges and limitations of this study

Throughout the completion of this project, we encountered various staining and imaging issues that are a common challenge for fluorescent antibody staining and imaging. Specifically, we experienced issues with certain samples or antibodies including auto-fluorescence, background fluorescence, non-specific binding, and poor tissue penetration (specifically for DAPI staining). Issues involving autofluorescence of debris or dislodged tissue were sometimes able to be resolved by washing to remove the debris, and then re-staining and re-imaging. We addressed the tissue penetration issue with DAPI by choosing to use a surface marker for segmentation instead of using DAPI, a nuclear marker. DAPI still gave us an outline of the overall tissue morphology which is useful for visualization. Addressing challenges related to background fluorescence or non-specific antibody binding involved reviewing the automated segmentation accuracy by examining high-resolution images containing the relevant markers. This helped determine which segmentation counts were accurate and, therefore, acceptable to use in the data analyses.

A challenge we encountered that relates to the imaging and staining issues discussed above is the detection of extracellular Granzyme B (GZMB). Typically, we would expect to find GZMB signal within the cell expressing it. However, we observed that most of the GZMB signals were outside of the cells, in the extracellular space surrounding the cytotoxic cells that most likely secreted the GZMB. According to [Boivin et al] extracellular GZMB concentration is expected to be much higher levels in inflamed tissue than it is in the blood. GZMB can cause more damage to tissues because of the abundance of ECM substrates for it to cleave. GZMB can be

found in the extracellular space for a number of reasons, including leakage from the immunological synapse during engagement for target cells. Additionally, *Lim et al 2023* show that accumulation of extracellular GZMB produced by NK cells is a driver of epithelial damage during HSV-2 vaginal infection.

The presence of extracellular GZMB is a challenge for using automated cell segmentation because that depends on the signal being overlayed semi-precisely with the cell in order to count that cell as positive for GZMB expression, and so on. As a result, it was clear that the segmentation algorithm was not associating much of the GZMB signal with the cell that produced it, for obvious and understandable reasons. In this case, the only thing left to do was examine the composite images by eye to get a better picture of how much GZMB expression there is compared to other samples and timepoints. While this is not quantitative as we would prefer, that is beyond the limit of the cell segmentation algorithms and it gives us more information than we had.

Additionally, we were limited by the number of subject samples able to be stained, imaged, and analyzed within the timeframe. A larger number of samples would broaden the statistical analyses and add power to them.

Significance

As emphasized throughout this paper, T cells are critical for controlling and eliminating localized HSV infection in the peripheral tissues. By decoding T cell functional states across skin healing in HSV-infected skin biopsies, we gain a more comprehensive understanding of the intricacies involved in orchestrating an effective immune response against chronic viral infections. Since T cells are susceptible to immune exhaustion resulting from constant antigen stimulation, finding ways to reinvigorate, or enhance, these dysfunctional cell populations could have a profound impact on finding efficacious treatments, and potentially a cure, for chronic recurrent infections such as HSV. Given T cells' susceptibility to immune exhaustion due to continuous antigen stimulation, revitalizing or enhancing these dysfunctional cell populations could significantly advance the search for effective treatments, and potentially a cure, for chronic recurrent infections such as HSV.

References

[1] Aleemardani M, Trikić MZ, Green NH, Claeyssens F. The Importance of Mimicking Dermal-Epidermal Junction for Skin Tissue Engineering: A Review. *Bioengineering (Basel)*. 2021;8(11):148. Published 2021 Oct 20. doi:10.3390/bioengineering8110148

[2] Anderson AC, Joller N, Kuchroo VK. Lag-3, Tim-3, and TIGIT: Co-inhibitory Receptors with Specialized Functions in Immune Regulation. Immunity. 2016;44(5):989-1004. doi:10.1016/j.immuni.2016.05.001

[3] Blackburn SD, Shin H, Haining WN, et al. Coregulation of CD8+ T cell exhaustion by multiple inhibitory receptors during chronic viral infection. *Nat Immunol.* 2009;10(1):29-37. doi:10.1038/ni.1679

[4] Boivin WA, Cooper DM, Hiebert PR, Granville DJ. Intracellular versus extracellular granzyme B in immunity and disease: challenging the dogma. Lab Invest. 2009;89(11):1195-1220. doi:10.1038/labinvest.2009.91

[5] Brown ZA, Wald A, Morrow RA, Selke S, Zeh J, Corey L. Effect of serologic status and cesarean delivery on transmission rates of herpes simplex virus from mother to infant. *JAMA*. 2003;289(2):203-209. doi:10.1001/jama.289.2.203

[6] Buggert M, Price DA, Mackay LK, Betts MR. Human circulating and tissue-resident memory CD8+ T cells [published correction appears in Nat Immunol. 2023 Sep;24(9):1591]. *Nat Immunol*. 2023;24(7):1076-1086. doi:10.1038/s41590-023-01538-6

[7] Celum C, Wald A, Hughes J, et al. Effect of aciclovir on HIV-1 acquisition in herpes simplex virus 2 seropositive women and men who have sex with men: a randomised, double-blind, placebo-controlled trial. *Lancet*. 2008;371(9630):2109-2119. doi:10.1016/S0140-6736(08)60920-4

[8] Corey L, Wald A, Celum CL, Quinn TC. The effects of herpes simplex virus-2 on HIV-1 acquisition and transmission: a review of two overlapping epidemics. *J Acquir Immune Defic Syndr*. 2004;35(5):435-445. doi:10.1097/00126334-200404150-00001

[9] Corey L, Wald A. Maternal and neonatal herpes simplex virus infections [published correction appears in N Engl J Med. 2009 Dec 31;361(27):2681]. *N Engl J Med*. 2009;361(14):1376-1385. doi:10.1056/NEJMra0807633

[10] Davé V, Richert-Spuhler LE, Arkatkar T, et al. Recurrent infection transiently expands human tissue T cells while maintaining long-term homeostasis. *J Exp Med*. 2023;220(9):e20210692. doi:10.1084/jem.20210692

[11] Donaghy H, Bosnjak L, Harman AN, et al. Role for plasmacytoid dendritic cells in the immune control of recurrent human herpes simplex virus infection. *J Virol*. 2009;83(4):1952-1961. doi:10.1128/JVI.01578-08

[12] Einhaus J, Rochwarger A, Mattern S, Gaudillière B, Schürch CM. High-multiplex tissue imaging in routine pathology-are we there yet?. *Virchows Arch*. 2023;482(5):801-812. doi:10.1007/s00428-023-03509-6

[13] Freeman EE, Weiss HA, Glynn JR, Cross PL, Whitworth JA, Hayes RJ. Herpes simplex virus 2 infection increases HIV acquisition in men and women: systematic review and meta-analysis of longitudinal studies. *AIDS*. 2006;20(1):73-83. doi:10.1097/01.aids.0000198081.09337.a7

[14] Galletti G, De Simone G, Mazza EMC, et al. Two subsets of stem-like CD8+ memory T cell progenitors with distinct fate commitments in humans. *Nat Immunol*. 2020;21(12):1552-1562. doi:10.1038/s41590-020-0791-5

[15] Gao Z, Feng Y, Xu J, Liang J. T-cell exhaustion in immune-mediated inflammatory diseases: New implications for immunotherapy. Front Immunol. 2022;13:977394. Published 2022 Sep 23. doi:10.3389/fimmu.2022.977394

[16] Goldberg MV, Drake CG. LAG-3 in Cancer Immunotherapy. *Curr Top Microbiol Immunol*. 2011;344:269-278. doi:10.1007/82_2010_114

[17] Gupta R, Warren T, Wald A. Genital herpes. *Lancet*. 2007;370(9605):2127-2137. doi:10.1016/S0140-6736(07)61908-4

[18] Han S, Phasouk K, Zhu J, Fong Y. Optimizing Deep Learning-Based Segmentation of Densely Packed Cells using Cell Surface Markers. Preprint. Res Sq. 2023;rs.3.rs-3307496. Published 2023 Sep 26. doi:10.21203/rs.3.rs-3307496/v1

[19] Hennig C, Adams N, Hansen G. A versatile platform for comprehensive chip-based explorative cytometry. Cytometry A. 2009;75(4):362-370. doi:10.1002/cyto.a.20668

[20] Herati RS, Knorr DA, Vella LA, et al. PD-1 directed immunotherapy alters Tfh and humoral immune responses to seasonal influenza vaccine. *Nat Immunol*. 2022;23(8):1183-1192. doi:10.1038/s41590-022-01274-3

[21] Herpes Simplex. Cleveland Clinic. Published May 17, 2022. Accessed December 9, 2023. https://my.clevelandclinic.org/health/diseases/22855-herpes-simplex

[22] Jarosch S, Köhlen J, Sarker RSJ, et al. Multiplexed imaging and automated signal quantification in formalin-fixed paraffin-embedded tissues by ChipCytometry. *Cell Rep Methods*. 2021;1(7):100104. Published 2021 Oct 27. doi:10.1016/j.crmeth.2021.100104

[23] Jarosch S, Köhlen J, Wagner S, D'Ippolito E, Busch DH. ChipCytometry for multiplexed detection of protein and mRNA markers on human FFPE tissue samples. *STAR Protoc*. 2022;3(2):101374. Published 2022 May 11. doi:10.1016/j.xpro.2022.101374

[24] Joller N, 2 AC, Kuchroo VK. LAG-3, TIM-3 and TIGIT: Distinct functions in immune regulation. *CellPress*. 2024;57(2):206-222. Published 2024 Feb 13. doi:10.1016/j.immuni.2024.01.010

[25] Kaye, KM. Genital Herpes. Merck Manuals. Published September 2021. Accessed December 2023. https://www.merckmanuals.com/professional/infectious-diseases/herpesviruses/genital-herpes

[26] Kim M, Truong NR, James V, et al. Relay of herpes simplex virus between Langerhans cells and dermal dendritic cells in human skin. *PLoS Pathog*. 2015;11(4):e1004812. Published 2015 Apr 13. doi:10.1371/journal.ppat.1004812

[27] Kortekaas Krohn I, Aerts JL, Breckpot K, et al. T-cell subsets in the skin and their role in inflammatory skin disorders. *Allergy*. 2022;77(3):827-842. doi:10.1111/all.15104

[28] Koutsky LA, Stevens CE, Holmes KK, Ashley RL, Kiviat NB, Critchlow CW, et al. Underdiagnosis of Genital Herpes by Current Clinical and Viral-Isolation Procedures. *N Engl J Med* (1992) 326(23):1533–9. doi: 10.1056/NEJM199206043262305

[29] Lei V, Petty AJ, Atwater AR, Wolfe SA, MacLeod AS. Skin Viral Infections: Host Antiviral Innate Immunity and Viral Immune Evasion. *Front Immunol*. 2020;11:593901. Published 2020 Nov 6. doi:10.3389/fimmu.2020.593901

[30] Lim YS, Lee AG, Jiang X, et al. NK cell-derived extracellular granzyme B drives epithelial ulceration during HSV-2 genital infection. *Cell Rep*. 2023;42(4):112410. doi:10.1016/j.celrep.2023.112410

[31] Lo M, Zhu J, Hansen SG, et al. Acute Infection and Subsequent Subclinical Reactivation of Herpes Simplex Virus 2 after Vaginal Inoculation of Rhesus Macaques. *J Virol*. 2019;93(2):e01574-18. Published 2019 Jan 4. doi:10.1128/JVI.01574-18

[32] Marcocci ME, Napoletani G, Protto V, et al. Herpes Simplex Virus-1 in the Brain: The Dark Side of a Sneaky Infection. *Trends Microbiol*. 2020;28(10):808-820. doi:10.1016/j.tim.2020.03.003

[33] Magaret AS, Wald A, Huang ML, Selke S, Corey L. Optimizing PCR Positivity Criterion for Detection of Herpes Simplex Virus DNA on Skin and Mucosa. *J Clin Microbiol.* (2007) 45(5):1618–20. doi: 10.1128/JCM.01405-06

[34] McLane LM, Abdel-Hakeem MS, Wherry EJ. CD8 T Cell Exhaustion During Chronic Viral Infection and Cancer. Annu Rev Immunol. 2019;37:457-495. doi:10.1146/annurev-immunol-041015-055318

[35] Milman N, Zhu J, Johnston C, et al. In Situ Detection of Regulatory T Cells in Human Genital Herpes Simplex Virus Type 2 (HSV-2) Reactivation and Their Influence on Spontaneous HSV-2 Reactivation. J Infect Dis. 2016;214(1):23-31. doi:10.1093/infdis/jiw091

[36] Murphy PR, Narayanan D, Kumari S. Methods to Identify Immune Cells in Tissues With a Focus on Skin as a Model. *Curr Protoc*. 2022;2(7):e485. doi:10.1002/cpz1.485

[37] Ohashi M, Bertke AS, Patel A, Krause PR. Spread of herpes simplex virus to the spinal cord is independent of spread to dorsal root ganglia. *J Virol*. 2011;85(6):3030-3032. doi:10.1128/JVI.02426-10

[38] Pachitariu M, Stringer C. Cellpose 2.0: how to train your own model. *Nat Methods*. 2022;19(12):1634-1641. doi:10.1038/s41592-022-01663-4

[39] Peng T, Phasouk K, Bossard E, et al. Distinct populations of antigen-specific tissue-resident CD8+ T cells in human cervix mucosa. *JCI Insight*. 2021;6(15):e149950. Published 2021 Aug 9. doi:10.1172/jci.insight.149950

[40] Peng T, Zhu J, Phasouk K, Koelle DM, Wald A, Corey L. An Effector Phenotype of CD8+ T Cells at the Junction Epithelium During Clinical Quiescence of Herpes Simplex Virus 2 Infection. *J Virol*. 2012;86(19):10587–96. doi: 10.1128/JVI.01237-12

[41] Peng T, Phasouk K, Sodroski CN, et al. Tissue-Resident-Memory $CD8^+$ T Cells Bridge Innate Immune Responses in Neighboring Epithelial Cells to Control Human Genital Herpes. *Front Immunol*. 2021;12:735643. Published 2021 Sep 6. doi:10.3389/fimmu.2021.735643

[42] Peng T, Zhu J, Klock A, et al. Evasion of the mucosal innate immune system by herpes simplex virus type 2. *J Virol*. 2009;83(23):12559-12568. doi:10.1128/JVI.00939-09

[43] Rha MS, Shin EC. Activation or exhaustion of $CD8^+$ T cells in patients with COVID-19. *Cell Mol Immunol*. 2021;18(10):2325-2333. doi:10.1038/s41423-021-00750-4

[44] Rosato PC, Beura LK, Masopust D. Tissue resident memory T cells and viral immunity. *Curr Opin Virol*. 2017;22:44-50. doi:10.1016/j.coviro.2016.11.011

[45] Roy S, Coulon PG, Prakash S, et al. Blockade of PD-1 and LAG-3 Immune Checkpoints Combined with Vaccination Restores the Function of Antiviral Tissue-Resident CD8+ TRM Cells and Reduces Ocular Herpes Simplex Infection and Disease in HLA Transgenic Rabbits. J Virol. 2019;93(18):e00827-19. Published 2019 Aug 28. doi:10.1128/JVI.00827-19

[46] Saeidi A, Zandi K, Cheok YY, et al. T-Cell Exhaustion in Chronic Infections: Reversing the State of Exhaustion and Reinvigorating Optimal Protective Immune Responses. Front Immunol. 2018;9:2569. Published 2018 Nov 9. doi:10.3389/fimmu.2018.02569

[47] Schiffer JT, Abu-Raddad L, Mark KE, et al. Mucosal host immune response predicts the severity and duration of herpes simplex virus-2 genital tract shedding episodes. Proc Natl Acad Sci U S A. 2010;107(44):18973-18978. doi:10.1073/pnas.1006614107

[48] Schildberg FA, Klein SR, Freeman GJ, Sharpe AH. Coinhibitory Pathways in the B7-CD28 Ligand-Receptor Family. *Immunity*. 2016;44(5):955-972. doi:10.1016/j.immuni.2016.05.002

[49] Schindelin J, Arganda-Carreras I, Frise E, et al. Fiji: an open-source platform for biological-image analysis. *Nat Methods*. 2012;9(7):676-682. Published 2012 Jun 28. doi:10.1038/nmeth.2019

[50] Schupp J, Christians A, Zimmer N, et al. In-Depth Immune-Oncology Studies of the Tumor Microenvironment in a Humanized Melanoma Mouse Model. Int J Mol Sci. 2021;22(3):1011. Published 2021 Jan 20. doi:10.3390/ijms22031011

[51] Schneider CA, Rasband WS, Eliceiri KW. NIH Image to ImageJ: 25 years of image analysis. *Nat Methods*. 2012;9(7):671-675. doi:10.1038/nmeth.2089

[52] Sheng W, Zhang C, Mohiuddin TM, et al. Multiplex Immunofluorescence: A Powerful Tool in Cancer Immunotherapy. *Int J Mol Sci*. 2023;24(4):3086. Published 2023 Feb 4. doi:10.3390/ijms24043086

[53] Sloan DD, Jerome KR. Herpes simplex virus remodels T-cell receptor signaling, resulting in p38-dependent selective synthesis of interleukin-10. *J Virol*. 2007;81(22):12504-12514. doi:10.1128/JVI.01111-07

[54] Stringer C, Wang T, Michaelos M, Pachitariu M. Cellpose: a generalist algorithm for cellular segmentation. *Nat Methods*. 2021;18(1):100-106. doi:10.1038/s41592-020-01018-x

[55] Tan WCC, Nerurkar SN, Cai HY, et al. Overview of multiplex immunohistochemistry/immunofluorescence techniques in the era of cancer immunotherapy. *Cancer Commun (Lond)*. 2020;40(4):135-153. doi:10.1002/cac2.12023

[56] Veenstra J, Dimitrion P, Yao Y, Zhou L, Ozog D, Mi QS. Research Techniques Made Simple: Use of Imaging Mass Cytometry for Dermatological Research and Clinical Applications. *J Invest Dermatol*. 2021;141(4):705-712.e1. doi:10.1016/j.jid.2020.12.008

[57] Wald A, Link K. Risk of human immunodeficiency virus infection in herpes simplex virus type 2-seropositive persons: a meta-analysis. *J Infect Dis*. 2002;185(1):45-52. doi:10.1086/338231

[58] Wald A, Zeh J, Selke S, Ashley RL, Corey L. Virologic characteristics of subclinical and symptomatic genital herpes infections. *N Engl J Med*. 1995;333(12):770-775. doi:10.1056/NEJM199509213331205

[59] Wald A, Zeh J, Selke S, et al. Reactivation of genital herpes simplex virus type 2 infection in asymptomatic seropositive persons. *N Engl J Med*. 2000;342(12):844-850. doi:10.1056/NEJM200003233421203

[60] Wolf Y, 2 AC, Kuchroo VK. TIM3 comes of age as an inhibitory receptor. *Nat Rev Immunol*. 2020;20(3):173-185. doi:10.1038/s41577-019-0224-6

[61] Wu Z, Zheng Y, Sheng J, et al. CD3+CD4-CD8- (Double-Negative) T Cells in Inflammation, Immune Disorders and Cancer. *Front Immunol*. 2022;13:816005. Published 2022 Feb 10. doi:10.3389/fimmu.2022.816005

[62] Yi JS, Cox MA, Zajac AJ. T-cell exhaustion: characteristics, causes and conversion. *Immunology*. 2010;129(4):474-481. doi:10.1111/j.1365-2567.2010.03255.x

[63] Yousef H, Alhajj M, Sharma S. Anatomy, Skin (Integument), Epidermis. In: *StatPearls*. Treasure Island (FL): StatPearls Publishing; November 14, 2022.

[64] Zhang J, Liu H, Wei B. Immune response of T cells during herpes simplex virus type 1 (HSV-1) infection. *J Zhejiang Univ Sci B*. 2017;18(4):277-288. doi:10.1631/jzus.B1600460

[65] Zhu J, Hladik F, Woodward A, et al. Persistence of HIV-1 receptor-positive cells after HSV-2 reactivation is a potential mechanism for increased HIV-1 acquisition. *Nat Med*. 2009;15(8):886-892. doi:10.1038/nm.2006

[66] Zhu J, Koelle DM, Cao J, et al. Virus-specific CD8+ T cells accumulate near sensory nerve endings in genital skin during subclinical HSV-2 reactivation. *J Exp Med*. 2007;204(3):595-603. doi:10.1084/jem.20061792

[67] Zhu J, Peng T, Johnston C, et al. Immune surveillance by CD8αα+ skin-resident T cells in human herpes virus infection [published correction appears in Nature. 2013 Aug 8;500(7461):242]. *Nature*. 2013;497(7450):494-497. doi:10.1038/nature12110